Cellular/Molecular

The Role of MAP1A Light Chain 2 in Synaptic Surface Retention of $Ca_V2.2$ Channels in Hippocampal Neurons

A. G. Miriam Leenders,[1] Lin Lin,[2] Li-Dong Huang,[2] Claudia Gerwin,[1] Pei-Hua Lu,[2] and Zu-Hang Sheng[1]

[1]Synaptic Function Section, The Porter Neuroscience Research Center, National Institute of Neurological Disorders and Stroke–National Institutes of Health, Bethesda, Maryland 20892-3701, and [2]Department of Neurobiology, Shanghai Jiao-Tong University School of Medicine, Shanghai 200025, China

$Ca_v2.2$ channels are localized at nerve terminals where they play a critical role in neurotransmission. However, the determinant that controls surface retention of these channels has not been identified. Here, we report that presynaptic surface localization of $Ca_v2.2$ is mediated through its interaction with light chain 2 (LC2) of microtubule-associated protein MAP1A. Deletion of a 23-residue binding domain within the $Ca_v2.2$ C terminus resulted in reduced synaptic distribution of the mutant channels. Using an antibody generated against an extracellular epitope of $Ca_v2.2$, we demonstrate that interfering the interaction with LC2 reduced surface expression of endogenous $Ca_v2.2$ at presynaptic boutons. In addition, the disruption of LC2–$Ca_v2.2$ coupling reduced Ca^{2+}-influx into nerve terminals through $Ca_v2.2$ and impaired activity-dependent FM4-64 uptake. The treatments of neurons with Latrunculin A to disrupt actin filaments resulted in reduced density of surface $Ca_v2.2$-positive boutons. Furthermore, LC2NT, a LC2 truncated mutant lacking the actin-binding domain, could not rescue $Ca_v2.2$ surface expression after suppressing LC2 expression with RNAi. Because actin filaments are major cytomatric components at the presynaptic boutons, these observations suggest a mechanism by which LC2 provides anchoring of surface $Ca_v2.2$ to the actin cytoskeleton, thus contributing to presynaptic function.

Key words: **calcium channels; presynaptic; surface expression; synaptic; axonal transport; microtubule; presynaptic regulation; actin**

Introduction

Calcium channels are multi-subunit complexes comprised of a major pore-forming $\alpha 1$ subunit ~250 kDa in size and smaller auxiliary β, $\alpha 2\delta$, and γ subunits (Catterall 2000). Of the multiple types of voltage-dependent calcium channels expressed in neurons (Ertel et al., 2000), two presynaptic calcium channels, $Ca_v2.1$ (P/Q-type) and $Ca_v2.2$ (N-type), are the primary Ca^{2+} entry pathways to support neurotransmitter release at central fast synapses (Dunlap et al., 1995; Lisman et al., 2007). The physical link between these presynaptic channels and SNARE proteins via the synprint region within the intracellular II–III loop of the channels provides close proximity between the Ca^{2+} entry site and the synaptic vesicle release machinery, allowing for rapid and efficient neurotransmitter release (Sheng et al., 1994, 1998; Stanley, 1997).

The synaptic localization of ion channels and receptors is likely determined by at least two mechanisms: initial sorting/targeting transport and later clustering/anchoring at the synaptic plasma membrane (Craig and Banker, 1994). Although the synprint region is implicated in presynaptic targeting of both $Ca_v2.1$ and $Ca_v2.2$ in superior cervical ganglion neurons (Mochida et al., 2003), it appears to be nonessential for polarized axonal trafficking in cultured hippocampal neurons (Szabo et al., 2006). The C terminus of $Ca_v2.2$ plays a critical role in channel synaptic targeting by binding to the active zone scaffolding proteins CASK and Mint1 (Maximov and Bezprozvanny, 2002) and to the motor dynein light chain subunit tctex1 (Lai et al., 2005). Recent observations suggest that CASK and $Ca_v2.2$ are colocalized at puncta within the nerve terminal cytoplasm, likely reflecting intracellular transport vesicles (Khanna et al., 2006). However, mechanisms underlying anchoring and retention of these channels at the presynaptic plasma membrane remain largely unknown. Recent findings established a role for the cytoskeleton in clustering neurotransmitter receptors and ion channels at synapses (Sheng and Pak, 2000; Lai and Jan, 2006). Physical connections between the actin cytoskeleton and voltage-gated ion channels are critical for proper localization of the channels. Such interactions include those between Na^+-channels and ankyrin (Bennett and Lambert, 1999), $K_v1.5$ and α-actinin (Maruoka et al., 2000), $K_v4.2$ and filamin (Petrecca et al., 2000), and $K_v1.2$ and cortactin (Hattan et al., 2002). However, it is unknown which, if any, cytoskeleton-associated elements may contribute to anchoring of voltage-gated calcium channels at the presynaptic surface.

Received July 2, 2008; revised Sept. 8, 2008; accepted Sept. 22, 2008.

This work was supported by the Chinese Young Scientist Foundation for International Collaboration Grant (399928001), the National Institute of Neurological Disorders and Stroke (NINDS) Intramural Competitive Fellowship Award (A.G.M. L.), and the Intramural Research Program of NINDS–National Institutes of Health (NIH) (Z.-H.S.). We thank Q. Cai and J.-S. Kang for their suggestions on live-cell imaging; Q. Cai and J. Stadler for help with hippocampal cultures; W. A. Catterall for CNB2 $Ca_v2.2$ antibody; I. Bezprozvanny for EGFP-$Ca_v2.2$ cDNA; S. Herlitze for pEGFP-$Ca_v2.1$ cDNA; C. Zyskind and D. Glazer-Schoenberg (NINDS) for editing; J. W. Nagle (DNA sequencing facility NINDS–NIH) for DNA sequencing; and S. Cheng and V. Tanner (EM facility NINDS–NIH) for their assistance with electron microscopy. A.G.M.L. conducted the majority of the cell biology and biochemical studies and manuscript writing; L.L., L.-D.H., and P.-H.L. performed yeast two-hybrid screening; and C.G. helped with biochemical analysis. Z.-H.S. is a senior author who was responsible for the project design and helped revise this manuscript.

The authors declare no competing financial interests.

Correspondence should be addressed to Zu-Hang Sheng, Synaptic Function Section, the Porter Neuroscience Research Center, National Institute of Neurological Disorders and Stroke–National Institutes of Health, Building 35, Room 3B203, 35 Convent Drive, Bethesda, MD 20892-3701. E-mail: shengz@ninds.nih.gov.

DOI:10.1523/JNEUROSCI.3078-08.2008

 0270-6474/08/2811333-14$15.00/0

Here, we report that MAP1A light chain 2 (LC2) serves as a binding partner for $Ca_v2.2$. LC2 is encoded on the MAP1A gene and generated by proteolytic cleavage from the MAP1A heavy chain (HC) (Hammarback et al., 1991; Langkopf et al., 1992). As part of the MAP1A complex, LC2 was first thought to play a role in stabilizing the cytoskeleton in mature neurons by promoting tubulin polymerization (Matus, 1988). LC2 also binds to microtubule (MT) or actin filaments independently of the MAP1A-HC (Tögel et al., 1998; Noiges et al., 2002) and acts as a binding partner for an orphan G-protein-coupled receptor (Maurer et al., 2004), the stargazin-AMPA receptor complex (Ives et al., 2004), and the BKCa potassium channel (Park et al., 2004). Our current study provides biochemical and cell biological evidence for a unique role of LC2 in anchoring $Ca_v2.2$ at the presynaptic surface, a process essential for activity-induced Ca^{2+}-influx into nerve terminals and subsequent neurotransmitter release.

Materials and Methods

Yeast two-hybrid screen. The C-terminal half (CT1, aa2046–2336) of rat $Ca_v2.2$ cDNA was inserted in frame into pGKBT7 bait vector containing the GAL4 DNA-binding domain. Yeast two-hybrid screens of a human brain cDNA library in vector pACT2 with the GAL4 activation domain were performed and evaluated according to the protocols described for the MATCH-MAKER yeast two-hybrid system (Clontech). Positive clones were selected on plates lacking leucine, tryptophan, histidine, and adenine with 50 mM 3-aminotriazole and confirmed by filter assay for b-galactosidase activity.

DNA constructs. Full-length and truncated mutants of LC2, $Ca_v2.2$, and $Ca_v2.1$ were subcloned into the pET28A (Novagen) and pGEX-4T-1 vectors (GE Healthcare). His- and GST-fusion proteins were prepared as bacterial lysates using BL21 (DE3) competent cells (one shot; Invitrogen) and purified as described previously (Ilardi et al., 1999; Lao et al., 2000). For mammalian expression, LC2, $Ca_v2.2$, and $Ca_v2.1$ constructs were subcloned into pcDNA3.1His (Invitrogen), pCMV-HA vector, pEGFP-C, pIRES-EGFP or pDsRed2-C (Clontech). Human $Ca_v2.2$ in pEGFP-C3 was kindly provided by Dr. I. Bezprozvanny (University of Texas Southwestern Medical Center, Dallas, TX), and $Ca_v2.1$ in pEGFP-C2 was kindly provided by Dr. S. Herlitze (Case Western Reserve University, Cleveland, OH). $Ca_v2.2$ mutant lacking binding domain (BD) (aa2046–2069) was constructed by linking the two PCR fragments of $Ca_v2.2$-CT (nt5448–6280) and (nt6353–7326) into pcDNA3.1His vector. This ΔBD fragment was then exchanged with CT1 in the full-length $Ca_v2.2$ by using *Xho*I and *Xba*I restriction sites.

siRNA. To design the siRNA duplex, three sequences unique to MAP1A HC and LC2 were selected from the open reading frame of rat MAP1A (NM_030995). siRNA1 corresponds to a HC coding sequence (nt3827–3847), siRNA2 and siRNA3 were against the LC2 coding sequences (nt8496–8512) and (nt8746–8766), respectively. Complementary oligonucleotides were annealed and inserted into the *Bam*HI/*Hin*dIII sites of pRNAT-H1.1/neo vector, a siRNA expression vector containing a GFP gene under a separate promoter for tracking transfected cells (GenScript).

Antibodies. Rabbit polyclonal anti-LC2 antibody was raised against the His-tagged N-terminal half of LC2. Rabbit polyclonal anti-$Ca_v2.2$ex antibody was raised against an extracellular peptide (aa1168–1183), the loop between IIIS1-S2 of the rat $Ca_v2.2$ (M92905). Both antisera were affinity purified using their antigenic peptides. Rabbit polyclonal $Ca_v2.2$in (Leenders et al., 2002) and goat polyclonal CNB2 (provided by Dr. Catterall, University of Washington, Seattle, WA) antibodies were raised against the rat $Ca_v2.2$ synprint region. Commercial monoclonal antibodies used included the following: synaptophysin (Millipore), Bassoon (Stessgen), CASK and MAP2 (BD Biosciences), PSD95 (Upstate), neuronal class III β-tubulin and HA.11 (Covance), actin (clone AC-40, Sigma), MAP1A (clone HM-1; Sigma) and β-tubulin (clone TUB 2.1; Sigma). Commercial polyclonal antibodies used included the following: GFP (ab6556) (Abcam), $Ca_v2.1$ (Alomone Labs) and goat polyclonal anti-synaptophysin (C-20) (Santa Cruz Biotechnology).

In vitro *binding experiments.* GST-fusion proteins were immobilized on glutathione-Sepharose beads (GE Healthcare). The bead-bound proteins were then incubated with His-protein lysates or transfected COS cell lysates in TBST (50 mM TBS, pH, 7.4, 0.1% Triton X-100) with protease inhibitors (1 mM phenyl-methylsulphonyl fluoride, 1 mM Leupeptin, and 1 mM Aprotinin) at 4°C for 3 h. After washing with TBST, bound complexes were separated by SDS-PAGE and immunoblotted with anti-T7 antibody (Novagen; EMD Biosciences). HRP-conjugated secondary antibodies and ECL chemiluminescence (GE HealthcareGE Healthcare) were used to visualize proteins. For sequential blotting, membranes were stripped between each antibody application in stripping buffer (62.5 mM Tris-HCl, pH 7.5, 20 mM DTT, and 1% SDS) at 50°C for 20 min.

Preparation of crude synaptosomes and synaptosomal fractions. Rat brain synaptosomes and fractionation were prepared as described previously (Leenders et al., 2004). Briefly, whole rat brains were homogenized in ice-cold sucrose buffer [320 mM sucrose, 1 mM EDTA, 5 mM Hepes, pH 7.4, supplemented with complete protease inhibitor mixture (Roche) and calpain inhibitor I and II (Sigma)]. Homogenates were centrifuged in a Sorvall centrifuge with an SS34 rotor at 3000 rpm for 10 min. The supernatant was placed on top of Percoll gradients (23, 15, 10, 3 in sucrose buffer) and spun in an SS34 rotor at 17,250 rpm for 5 min. Crude synaptosomes were collected from the interface between the 15 and 23% gradients, mixed with sucrose buffer, and then pelleted in an SS34 rotor at 13,000 rpm for 15 min. For fractionation, crude synaptosomes were washed once in medium M (0.32 M sucrose, 1 mM K_2HPO_4, 0.1 mM EDTA, pH 7.5), resuspended and homogenized in medium L (1 mM K_2HPO_4, 0.1 mM EDTA, pH 8.0), and layered over 5 ml of 1 M sucrose in medium L and then centrifuged for 30 min at 96,300 × *g* in an SW27 rotor. The supernatant was mixed to homogeneity and centrifuged again for 14 h at 25,000 × *g*. The supernatant was collected as synaptic cytosol, and the pellets were homogenized in medium L and applied to a gradient of 7 ml 1.2, 1.0, 0.8, 0.6, and 0.4 M sucrose in medium L and centrifuged for 90 min at 68,000 × *g* in an SW27 rotor. Bands at each interface were collected. The band above the 0.4 M sucrose layer contained enriched synaptic vesicles (SV), and the band from the interface 0.8/1.0 M contained mostly enriched plasma membranes (PM). The SV and PM fractions were further washed once and pelleted with medium L in a Ti50 rotor (45 min at 106,500 × *g*). The synaptic cytosol was dialyzed against medium L and centrifuged at 140,000 × *g* in a Ti 50 rotor for 1 h to separate any remaining synaptic vesicles from soluble proteins. For PSD fraction, PM was diluted in 50 mM Hepes, 2 mM EDTA and 0.5% Triton X-100, and followed by centrifugation at 32,000 × *g* in SS34 rotor. All pellets were resuspended in 20 mM Tris-HCl, pH 7.5. Protein concentration in each fraction was determined by protein assay using BSA as standard.

Coimmunoprecipitation. Proteins from synaptosomal preparations or P2 rat brain homogenates were solubilized with 1% 3-[(3-cholamidopropyl)-dimethylammonio]-1-propane sulfonate in sucrose buffer for 1 h at 4°C, and insoluble material was cleared by centrifugation for 30 min at 4°C. Solubilized proteins (100–300 μg) were mixed with primary antibodies, or, as control, rabbit normal IgG (Invitrogen) and 2.5 mg Protein A-Sepharose CL-4B resin (GE Healthcare) in 0.5 ml PBS with protease inhibitor mixture and calpain inhibitor I and II, and then incubated on a microtube rotator overnight at 4°C, followed by three washes with PBS. Detection of immunoprecipitated proteins was performed by SDS-PAGE and immunoblotting.

Immuno-electron microscopy analysis. Adult male Sprague–Dawley rats (250 g) under isoflurane anesthesia were perfused transcardially with 10 U/ml heparin in PBS followed by a mixture of 4% paraformaldehyde (Aldrich) and 0.9% picric acid (Sigma) in 0.1 M phosphate buffer, pH 7.4. The brain was removed and postfixed in the same buffer overnight. Coronal slices (20 μm) were sectioned on a sliding vibratome and permeabilized with PBS containing 5% goat serum, and 0.04% saponin for 1 h, and then stained with anti-LC2 affinity-purified antibody at 1:250. After washing, the brain slices were incubated in PBS containing 5% low-fat milk and 5 μl Nanogold-labeled anti-rabbit antibody (Nanoprobe), followed by fixation with 2% glutaraldehyde in PBS for 30 min. The brain slices were silver enhanced (HQ silver enhancement kit; Nano-

probe) for 4 min, treated with 0.2% osmium tetroxide in 0.1 M phosphate buffer for 30 min, and then processed for electron microscopy.

Transfection and immunocytochemistry of hippocampal neurons. Rat hippocampal neuron cultures were prepared from hippocampi dissected from embryonic day 18 (E18) or E19 rat embryos as described (Goslin et al., 1998) and plated at a density of 100,000 cells/12 mm coverslips coated with polyornithine and fibronectin in a 20:80 mix of glial feed (10% FBS in Neurobasal; Invitrogen) and neuronal feed (Neurobasal supplemented with B27 and L-glutamine). Starting at 2–3 days *in vitro* (DIV), cultures were maintained in conditioned medium with half-feed changes of neuronal feed lacking glutamine every 3–4 d. Neurons were transfected using Calcium-Phosphate (BD Biosciences) method at 7–9 DIV. For each coverslip a maximum of 6 μg DNA was combined with 6 μl calcium solution (2 M) in a total of 50 μl H_2O. This DNA/calcium mixture was added drop-wise to 50 μl 2× HBS solution and incubated for 20 min at room temperature (RT) before added to neurons for 20–30 min. For immunofluorescent staining, cultured cells were fixed with 4% sucrose/4% paraformaldehyde in PBS at RT for 10 min or in prechilled 100% methanol at −20°C for 10 min, washed three times in PBS for 5 min, permeabilized in 0.2% Saponin for 5 min, and blocked in 5% normal goat or donkey serum in PBS for 1 h. Fixed cultures were incubated with primary antibodies in PBS/5% serum and 0.05% saponin overnight at 4°C or for 2 h at RT. For surface $Ca_v2.2$ s staining, fixed neurons were blocked but not permeabilized, then incubated with anti-$Ca_v2.2$ex antibody overnight, followed by permeabilization and synaptophysin staining. After primary antibody incubations, the cells were washed four times in PBS at RT for 5 min each, incubated with secondary Alexa fluorescent antibodies (Invitrogen) at 1:400 dilution in PBS/5% serum and 0.05% saponin for 30 min at RT, washed again with PBS, mounted with antifade mounting medium, and imaged using a Zeiss LSM 510 oil-immersion 40× objective with a sequential-acquisition setting. For quantification of the fluorescence signals, images were acquired by using the same settings below saturation at a resolution of 1024 × 1024 pixels (12 bit). Four to six sections were taken from top-to-bottom of the specimen and the brightest point projections were made. The selected images were then exported to Adobe Photoshop and/or NIH ImageJ. Transfected neurons were chosen for quantification from at least three independent experiments for each condition. For synaptic targeting measurements of GFP–$Ca_v2.2$ or GFP–$Ca_v2.1$, transfected axons were identified based on morphology or absence of dendritic marker MAP2 staining, and randomly selected, usually at least 100 μm away from the cell body, and manually traced. Synaptic boutons were identified based on synaptophysin puncta along the traced axon; mean intensities of synaptophysin and GFP signals were measured with a particle analyzing function in NIH ImageJ, with parameters set to include only puncta ranging between 0.25–2 μm in diameter mean intensities for synaptic puncta and axon were automatically scored and obtained by the software. For synaptic clustering of GFP–$Ca_v2.2$, mean fluorescent signal at boutons were calculated relative to that from traced axons and expressed as fluorescent intensity ratio: $I_{synapse}/I_{axon}$. To evaluate surface density of endogenous $Ca_v2.2$, neurons were immunostained with anti-$Ca_v2.2$ex antibody before membrane permeabilization. Images were imported into ImageJ and transfected axons were manually traced on the basis of GFP fluorescence, which creates a mask to generate separate images for transfected and untransfected neuronal processes. The mean fluorescent intensity of surface $Ca_v2.2$ s at presynaptic boutons colabeled by synaptophysin was calculated with particle analyze function in ImageJ set to include puncta of 0.25–2 μm in diameter and then automatically scored. Measured data were expressed as normalized mean fluorescence intensity of boutons from transfected neurons relative to that from the untransfected cells.

Live imaging of presynaptic Ca^{2+}-transients with Fluo-4NW. Neurons were cotransfected with DsRed-monomer-synaptophysin and GFP or GFP-BD at 7–9 DIV; imaging was performed at 13–16 DIV on a Zeiss LSM 510 confocal microscope with a 40 × C apochromatic water-immersion lens (1.2 NA). Calcium imaging was performed using Fluo-4NW dye (Invitrogen) in modified Tyrode's solution [(in mM) 145 NaCl, 3 KCl, 1.2 $MgCl_2$,2.4 $CaCl_2$, 10 Glucose, 10 HEPES, and 0.5 kynurenic acid, pH7.4] supplemented with 2.5 mM Probenecid (Invitrogen) to inhibit Fluo-4NW extrusion. Fluorescence of Fluo-4NW and DsRed-synaptophysin was excited at 488 and 543 nm, respectively. The lowest intensity of lasers and the shortest scanning time were used; pinhole openings were set for 2 μm depth of optical slice. Time-lapse images for one to three boutons were collected at 100 × 30 pixels resolution (12 bit) and taken at 20 Hz (scan time <50 ms) to meet Nyquist sampling rate for 10 Hz stimulation, which was generated with a Master 8 stimulator (AMPI) and amplified with an A385 World Precision Instruments Stimulus Isolator. Thirty biphasic pulses at 10 Hz were delivered through platinum electrodes positioned on opposite sides of the field stimulation chamber (18.0 × 6.3 × 2.3 mm; Warner) at 1 ms of stimulus duration and 50 mA constant current. Calcium images were analyzed using the image stack function "Plot *z*-axis Profile" of ImageJ (NIH). Baseline (F_0) intensity was averaged from 40 images before stimulus and changes in fluorescence were calculated relative to the baseline and expressed as percentage of $\Delta F/F_0 = [(F - F_0)/F_0] \times 100$. Peak values were calculated by averaging the last 20 frames during stimulation. After measuring control Ca^{2+}-transient, when applicable, Ca^{2+}-channel toxins ω-Conotoxin GVIA (1 μM) and ω-Agatoxin IVA (100 nM) were applied in Tyrode's solution for 10 min followed by acquisition of a second Ca^{2+}-transient. Percentage inhibition by toxins was calculated as relative value of Ca^{2+}-transient before toxin application from the same boutons.

Functional labeling of presynaptic boutons with FM4-64. Neurons were transfected with GFP-IRES-siRNA at 7–9 DIV and imaging was performed at 13–16 DIV. Presynaptic terminals were loaded with 15 mM fluorescent styryl dye FM 4–64 (*N*-(3-triethylammoniumpropyl)-4-(*p*-dibutylaminostyryl) pyridinium, dibromide) (Invitrogen) in a high K^+ solution containing the following (in mM): 95 NaCl, 50 KCl, 10 glucose, 10 HEPES, 1.2 $CaCl_2$, 1.2 $MgCl_2$, and 0.5 kynurenic acid, pH7.4, for 2 min at RT and washed for 30 min with a calcium-free Tyrode's solution (in mM: 145 NaCl, 3 KCl, 1.2 $MgCl_2$,10 Glucose and 10 HEPES, pH7.4) to remove nonspecific membrane-bound FM4-64. Images covering both transfected and untransfected axon processes were collected before and after unloading (5 min) in high K^+ perfusion. Activity-dependent uptake of FM4-64 dye was obtained by subtracting the unloading image from the loading image. Average fluorescence intensities were measured from individual puncta (at least 1.0 × 1.0 mm^2) traced along the axons of transfected and untransfected neurons. When applicable, after capturing the first set of images Ca^{2+}-channel toxins ω-Conotoxin GVIA (1 μM) and ω-Agatoxin IVA (100 nM) were applied in Tyrode solution for 10 min followed by a second set of image acquisition. Imaging was performed using a confocal microscope (Zeiss; LSM 510) with a 40 × C apochromatic water-immersion lens (1.2 NA). Fluorescence of GFP and FM dye was excited at 488 and 543 nm, respectively. All images were collected at 1024 × 1024 pixel resolution and 2.0–4.0 × software zoom.

Results

$Ca_v2.2$ selectively interacts with LC2

To identify proteins involved in presynaptic surface expression of $Ca_v2.2$, we performed a yeast two-hybrid screen with the $Ca_v2.2$ cytoplasmic C-terminal domain (CT1, aa2046–2336) as bait (Fig. 1*A*). Screening of a human brain cDNA library led to isolating 76 clones encoding 25 cDNA genes. In addition to motor dynein (1 clone), Mint 1 (3 clones), and neurexin 3 (2 clones), we identified 33 clones encoding overlapping sequences of LC2 from MAP1A and one clone encoding LC1 of MAP1B (Fig. 1*B*). MAP1A and MAP1B are MT-associated proteins expressed in developing (MAP1B) and mature (MAP1A) neurons (Matus, 1988). Because both LC1 and LC2 associate with the MT and actin cytoskeleton (Tögel et al., 1998; Noiges et al., 2002) and bind several membrane proteins (Ives et al., 2004; Maurer et al., 2004; Park et al., 2004), we investigated a possible involvement in the surface localization of $Ca_v2.2$ at synapses. Given that the yeast two-hybrid screen isolated 33 LC2 clones versus one LC1 clone and that LC2 is more abundant in mature neurons where $Ca_v2.2$ predominantly localizes at synapses, we selected LC2 for further characterization.

To confirm the interaction between LC2 and $Ca_v2.2$ via its

CT1 domain, we first performed pull-down studies using GST-tagged LC2 proteins. His-$Ca_v2.2$-CT1 selectively interacted with GST-LC2 and GST-LC2-NT, the N-terminal half of LC2, whereas no interaction was observed with GST-LC2-CT (C-terminal half) or GST alone (Fig. 1*C*). Next, we performed immunoprecipitation to examine LC2-$Ca_v2.2$ complex in neurons. An anti-$Ca_v2.2$ antibody could coprecipitate $Ca_v2.2$ and LC2 from rat brain homogenates (Fig. 1*D*). Conversely, an anti-LC2 antibody coprecipitated $Ca_v2.2$ but not $Ca_v2.1$ from synaptosomal preparation, a synaptic terminal-enriched fraction (Fig. 1*E*), suggesting the selective interaction of LC2 with the $Ca_v2.2$ channels. Using GST-fusion constructs with different $Ca_v2.2$ C-terminal fragments, we further mapped the LC2-binding sequence (BD) to 23 residues (CT2, aa2046–2069) (Fig. 1*F*,*G*). The sequence of BD in $Ca_v2.2$ shares a low homology (36%) with the corresponding region of $Ca_v2.1$, suggesting that BD is specific for the $Ca_v2.2$ channels. The efficacy of BD in its binding to LC2 was further tested by immunoprecipitation using lysates from transfected COS-7 cells. Both the GFP-BD and GFP-$Ca_v2.2$-CT could coprecipitate HA-LC2 (Fig. 1*H*). In contrast, expression of either GFP or GFP-CTΔBD mutant alone or coexpression of BD with $Ca_v2.2$-CT failed to precipitate HA-LC2. Consistent with the findings in synaptosomal preparations (Fig. 1*E*), no binding was detected between GFP-$Ca_v2.1$-CT and HA-LC2 (Fig. 1*H*). Thus, our studies suggest that $Ca_v2.2$ selectively interacts with LC2 via its LC2-binding domain within the C terminus.

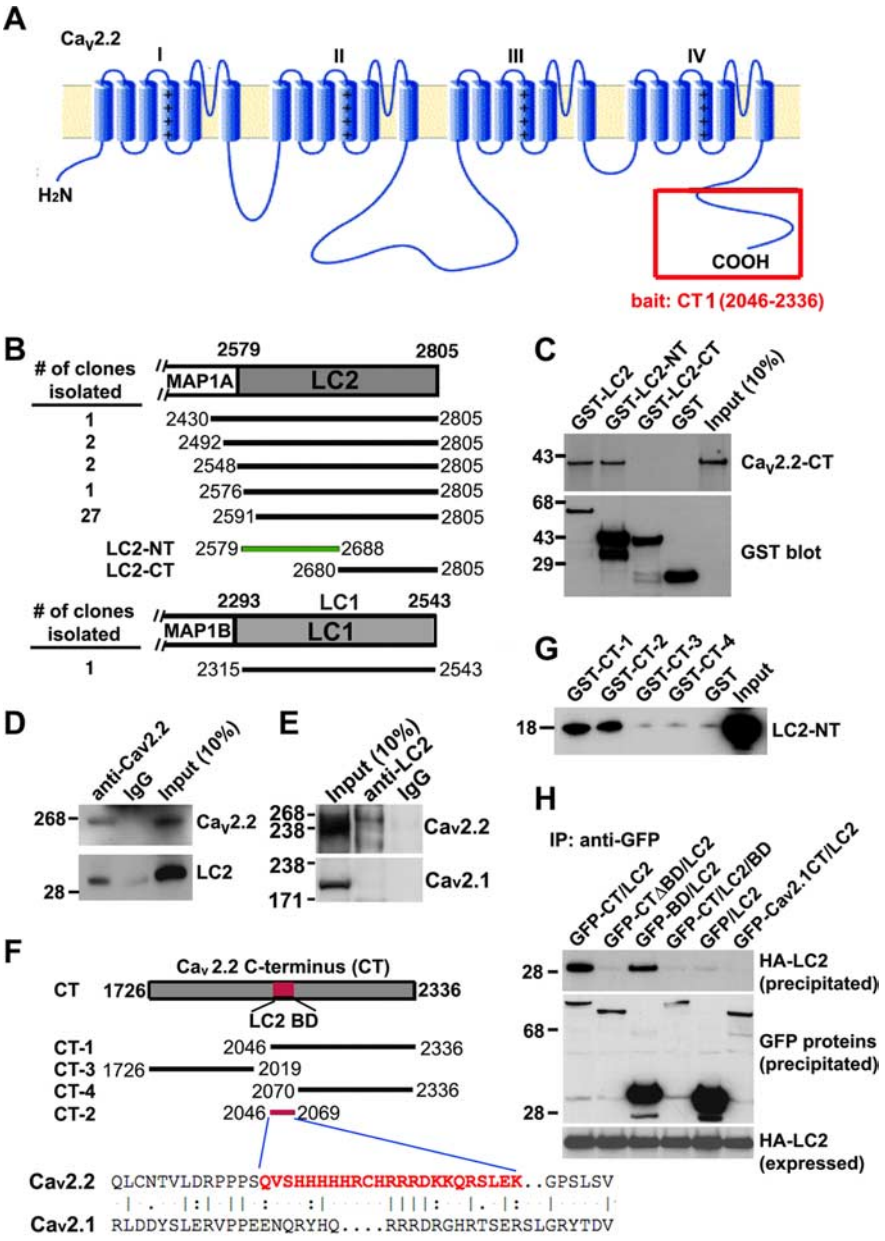

Figure 1. Selective interaction between $Ca_v2.2$ and LC2. ***A***, Schematic representation of $\alpha 1$ subunit of the $Ca_v2.2$ channels. Red box indicates the C-terminal fragment CT1 (aa2046–2336) of rat $Ca_v2.2$ cDNA used as bait in the yeast two-hybrid system. ***B***, LC1 and LC2 clones isolated in the yeast two-hybrid screen. ***C***, *In vitro* binding experiments. GST-fusion proteins immobilized on glutathione-Sepharose beads were incubated with His-tagged $Ca_v2.2$-CT1. Bound proteins were analyzed by Western blotting using antibodies against T7-tag (top) and GST (bottom). The N-terminal half (aa2579–2688) of LC2 (green bar in ***B***) is required for its interaction with $Ca_v2.2$-CT. ***D***, Immunoprecipitation from rat brain homogenates using anti-$Ca_v2.2$ antibody followed by Western blots for $Ca_v2.2$ (top) and LC2 (bottom). ***E***, Immunoprecipitation from rat brain synaptosomal preparations with anti-LC2 antibody followed by Western blots of $Ca_v2.2$ (top) and $Ca_v2.1$ (bottom). ***F***, ***G***, Schematic representation (***F***) and pull-down assay (***G***) of His-tagged LC2-NT with truncated GST-$Ca_v2.2$-CT fusion proteins. CT-2 (aa2046–2069), shown as a red bar in ***F***, is the LC2-BD on $Ca_v2.2$ C terminus. ***H***, BD interferes with the interaction between GFP-$Ca_v2.2$-CT and HA-LC2 in COS-7 cells. Immunoprecipitation (IP) of the complex from lysates was performed 48 h after transfection with anti-GFP antibody. Precipitated proteins were detected with anti-HA (top and bottom) and anti-GFP (middle) antibodies.

LC2 colocalizes with $Ca_v2.2$ at presynaptic terminals

MAP1A is important for maintaining the MT cytoskeleton in axons as well as dendrites (Matus, 1988). However, synaptic localization of either MAP1A-HC or LC2 at central synapses has not been investigated. We performed three lines of experiments to examine the presence of LC2 at synaptic sites. First, we made subcellular fractionations from rat cerebral crude synaptosomes into cytosol, synaptic vesicles, synaptic plasma membrane, and postsynaptic density (PSD). These fractions were then analyzed by sequential immunoblotting with antibodies against LC2, MAP1A-HC, β-tubulin, actin, and markers for each fraction including Na-K-ATPase (plasma membrane), synaptophysin (synaptic vesicles), α/β-SNAP (cytosol), and PSD95 (PSD). LC2 is relatively enriched in the plasma membrane-associated fraction of synaptic terminals, whereas MAP1A-HC, together with β-tubulin and actin, is present primarily in the cytosolic fraction (Fig. 2*A*). In addition, although both PSD95 and LC2 are detected in the PSD fraction, PSD95 is much more enriched, whereas LC2 is less abundant compared with the crude synaptosomal preparations (Fig. 2*B*). Next, we sought to determine the distribution of LC2 at presynaptic terminals in more detail by immuno-electron microscopy of perfusion fixed brain tissue. LC2 was observed adjacent to the plasma membrane near or at the active zones or near the postsynaptic density (Fig. 2*C*). Furthermore, subcellular distribution of LC2 in neurons was ex-

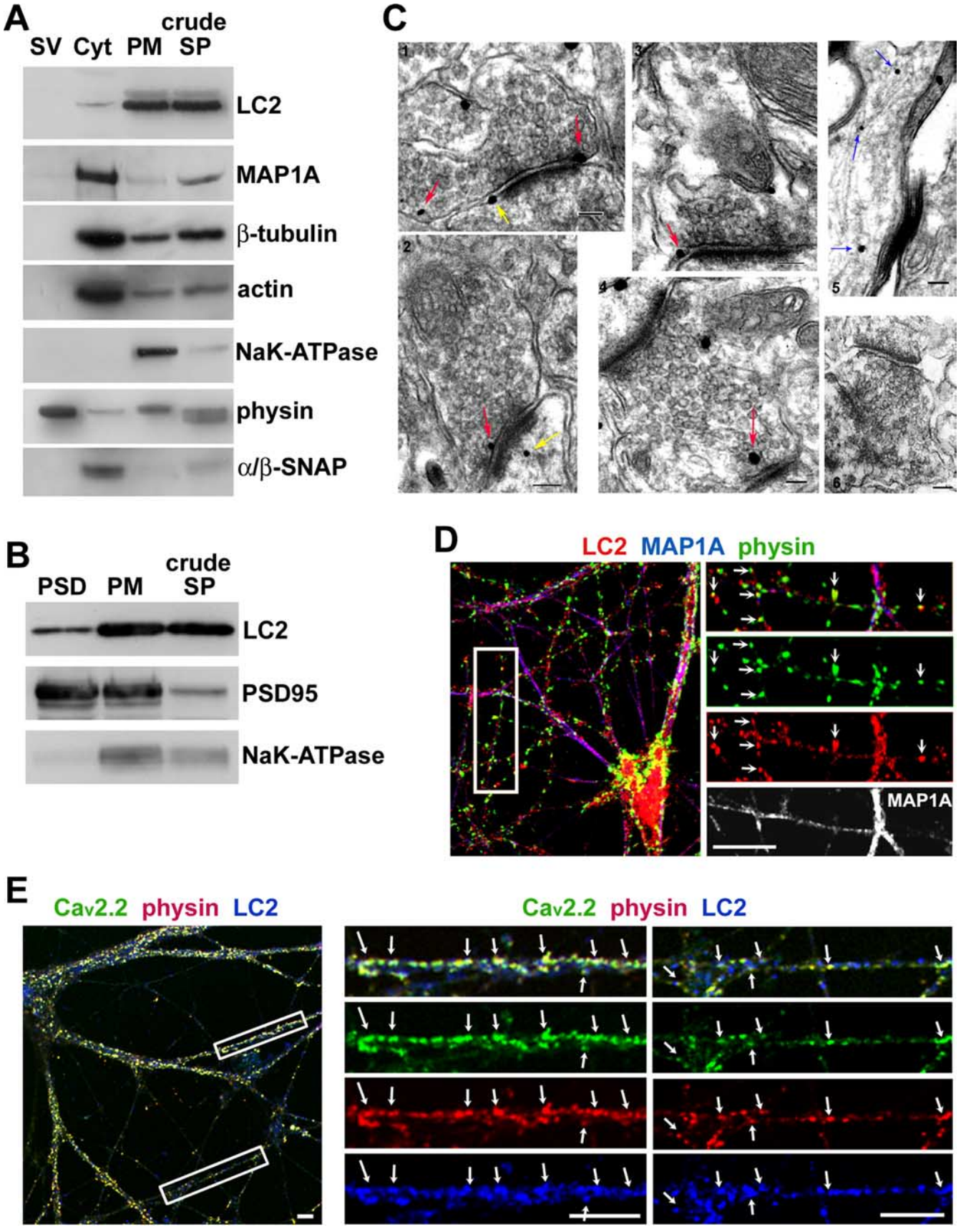

Figure 2. LC2 is present at the presynaptic terminals. ***A***, ***B***, Western blot analysis of equal amounts (10 μg) of SV, cytosol (Cyt), PM, and PSD fractions from rat brain synaptosomal preparations (crude SP). ***A***, ***B***, LC2 is relatively enriched in the PM fraction of synaptosomes (***A***), not in the PSD fraction (***B***), whereas MAP1A-HC is predominantly found in the cytosolic fraction along with β-tubulin and actin. Relative purity of the fractions was assessed with markers for each fraction: synaptophysin (SV), α/β-SNAP (Cyt), PSD95 (PSD), and Na-K-ATPase (PM). ***C***, Immunostaining LC2 under electron microscopy of perfused rat brain cortex slices. Immunogold-labeled LC2 is observed near the presynaptic membrane of the active zone (red arrows) (*Figure legend continues*.)

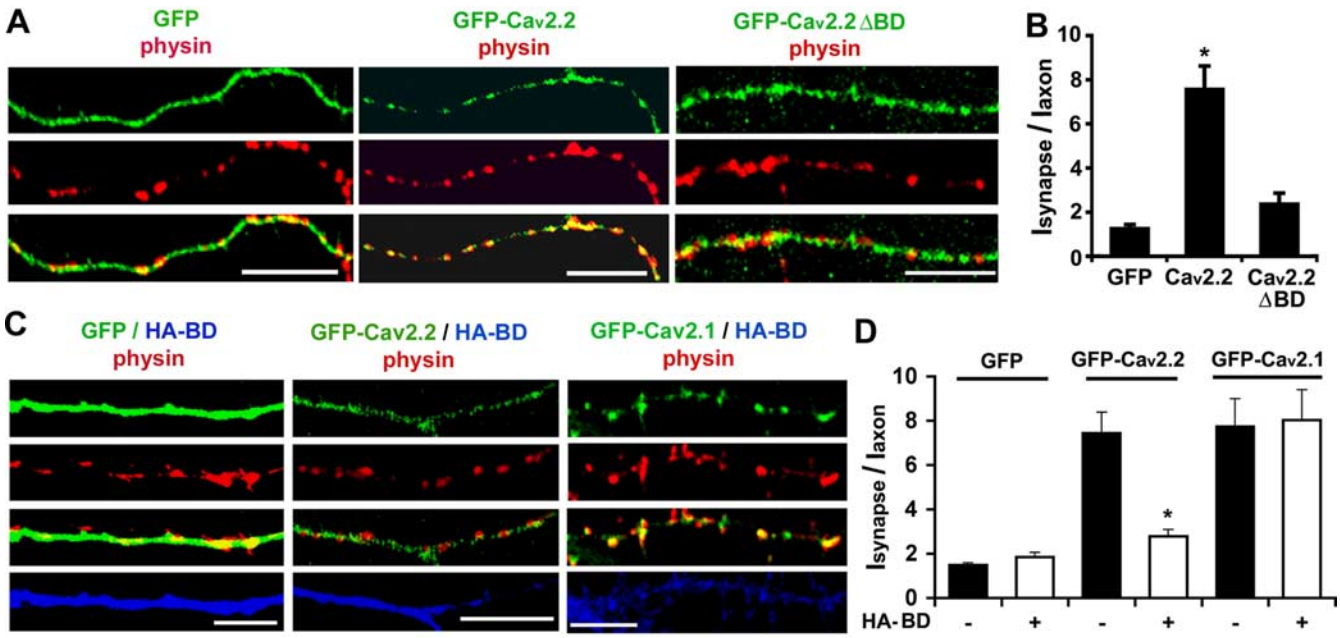

Figure 3. BD is important for synaptic localization of GFP–$Ca_v2.2$. ***A***, Deletion of BD from $Ca_v2.2$ impaired synaptic localization of the channels. Representative images of axonal segments of hippocampal neurons expressing GFP–$Ca_v2.2$, GFP–$Ca_v2.2\Delta$BD, or GFP at 7–9 DIV, followed by immunostaining at 14 DIV for GFP (green) and synaptophysin (red). ***B***, Relative ratio of GFP fluorescence intensity at synapses over axons ($I_{synapse}/I_{axon}$). Total axon length measured is 1020 μm (GFP), 1116 μm ($Ca_v2.2$), and 993 μm ($Ca_v2.2\Delta$BD), respectively. ***C***, Representative axonal images of hippocampal neurons coexpressing HA-BD with GFP, GFP–$Ca_v2.2$, or GFP–$Ca_v2.1$ at 7–9 DIV and immunostained for GFP (green), synaptophysin (red), and HA (blue) at 14 DIV. ***D***, Relative ratio of GFP fluorescence intensity at synapses over axons revealed that coexpression of HA-BD selectively reduced synaptic targeting of $Ca_v2.2$ but not $Ca_v2.1$. Total axon length measured was 1020 μm (GFP), 754 μm (GFP + HA-BD), 1116 μm ($Ca_v2.2$), and 987 μm ($Ca_v2.2$ + HA-BD), 1050 μm ($Ca_v2.1$) and 1088 μm ($Ca_v2.1$ + HA-BD). Data are means ± SEM; $n = >300$ synaptic puncta pooled from 10 neurons of at least three separate cultures (*$p < 0.001$ by Student's t test). Scale bars, 10 μm.

amined in low-density hippocampal cultures. LC2, together with MAP1A-HC, was present in the cell body and neuronal processes. However, unlike MAP1A-HC that mainly localized along processes, LC2 was also detected as punctate staining colocalized with the synaptic marker synaptophysin and $Ca_v2.2$ (Fig. 2*D*,*E*).

BD is required for the synaptic localization of $Ca_v2.2$

To explore the physiological relevance of the interaction between LC2 and $Ca_v2.2$, we analyzed the synaptic localization of GFP-tagged $Ca_v2.2$ or its mutant expressed in cultured neurons. The neurons were transfected at 7–9 DIV followed by coimmunostaining for synaptophysin and GFP at 14 DIV. Given limited synaptic targeting slots for Ca_vs (Cao et al., 2004), which might cause mistargeting of overexpressed GFP-$Ca_v2.2$, we selected the neurons with low and moderate expression of the channels and visualized GFP-$Ca_v2.2$ signal in the distal axons by immunostaining of GFP antibody. In contrast to GFP control, GFP-$Ca_v2.2$ was mainly observed as punctate staining along the axon, where most (~70%) of synaptophysin puncta from the transfected neurons displayed a detectable GFP-$Ca_v2.2$ signal, indicating synaptic localization (Fig. 3*A*). This distribution pattern was similar to that found for exogenously expressed $Ca_v2.2$ in neurons (Maximov and Bezprozvanny, 2002; Szabo et al., 2006). In considering possible saturation of the limited targeting slots for Ca_vs (Cao et al., 2004) by expressed GFP-$Ca_v2.2$, analysis of synaptic colocalization would be less sensitive to measure any minor defects in synaptic targeting. To more accurately reflect changes in relative distribution of GFP-$Ca_v2.2$, we instead measured mean intensity ratio of GFP-$Ca_v2.2$ at synapses versus in axons. Quantitative analysis showed a remarkably higher mean intensity of GFP-$Ca_v2.2$ at synapses over that in the axons ($I_{synapse}/I_{axon}$ ratio: 7.4 ± 0.9), whereas GFP was more evenly distributed in both compartments ($I_{synapse}/I_{axon}$ ratio: 1.5 ± 0.1) (Fig. 3*B*). To investigate the potential role of the $Ca_v2.2$-LC2 interaction in the channel targeting, we constructed a GFP-$Ca_v2.2$ mutant lacking BD. Although GFP-$Ca_v2.2\Delta$BD was present in the axons, it was significantly reduced in synaptic clustering ($I_{synapse}/I_{axon}$ ratio: 2.3 ± 0.4).

To further confirm the role of BD in channel targeting, we coexpressed this binding domain transgene with GFP-$Ca_v2.2$ in hippocampal neurons (Fig. 3*C*). Consistent with its competitively inhibitory role in immunoprecipitation of LC2 with $Ca_v2.2$ in the transfected COS-7 cells (Fig. 1*H*), coexpression of HA-BD markedly reduced the synaptic localization of GFP-$Ca_v2.2$ ($I_{synapse}/I_{axon}$ ratio: 2.8 ± 1.4, $p < 0.001$) (Fig. 3*C*,*D*). Similar to the deletion mutant of the channel, GFP-$Ca_v2.2$ was rather diffuse throughout the axon and less clustered within synapses when HA-BD was coexpressed. $Ca_v2.1$ is another predominant Ca_v2 channel involved in presynaptic transmission at central synapses. However coexpression of HA-BD had no effect on the synaptic targeting of GFP-$Ca_v2.1$ ($I_{synapse}/I_{axon}$ ratio: 7.7 ± 1.3 for $Ca_v2.1$+HA and 8.0 ± 1.4 for $Ca_v2.1$+HA-BD, $n = 20$, $p = 0.87$) (Fig. 3*E*,*F*), suggesting that LC2 played a role in synaptic localization specific for the $Ca_v2.2$ channels.

←

(*Figure legend continued*.) and postsynaptic localization (yellow arrows) (***C1–4***), and along microtubules in neuronal processes (blue arrows; ***C5***). As a control, immunogold was not found at synapses in the absence of anti-LC2 antibody (***C6***). Scale bars, 100 nm. ***D***, Distribution of LC2 in low-density cultures of E18 rat hippocampal neurons at 14 DIV. LC2 appears as punctate staining along neuronal processes and partially colocalizes with synaptophysin (physin) puncta (white arrows). The right panels in ***D*** are the close-up views of the boxed region. ***E***, Synaptic colocalization of LC2 with $Ca_v2.2$ in hippocampal neurons (14 DIV). The middle and right panels are the close-up views of the boxed regions showing colocalization of LC2 (blue) and $Ca_v2.2$ (green) at synaptophysin puncta (red) along neuronal processes. Scale bars: ***D***, ***E***, 10 μm.

Because binding of $Ca_v2.2$ channels with CASK and MINT via its C-terminal domains also contributed to synaptic targeting (Maximov and Bezprozvanny, 2002), we sought to test whether reduced synaptic clustering by deleting the BD sequence could be attributed to the impaired binding of these two proteins to the $Ca_v2.2$ channels. First, pull-downs and immunoprecipitations demonstrated that deleting BD from the $Ca_v2.2$ C-terminal did not abolish its interactions with CASK and MINT1 (supplemental Fig. S1*A*,*B*, available at www.jneurosci.org as supplemental material). The SH3-binding domain (2188–2199) within the $Ca_v2.2$ C-terminal is the CASK-binding sequence, which is located near but does not overlap the BD (2046–2069). Second, the GFP-$Ca_v2.2$ mutant lacking BD alone ($I_{synapse}/I_{axon}$ ratio: 2.45 ± 0.3, $p < 0.001$) or both BD and SH3-binding domain ($I_{synapse}/I_{axon}$ ratio: 1.7 ± 0.1, $n = 15$, $p < 0.001$) had a more profound defect in synaptic clustering compared with wild-type control ($I_{synapse}/I_{axon}$ ratio: 9.2 ± 0.8, $n = 15$) (supplemental Fig. S1*C*,*D*, available at www.jneurosci.org as supplemental material). However, the neurons transfected with GFP-$Ca_v2.2$ mutant lacking the SH3-binding domain can be divided into two groups: one displayed reduced clustering ($I_{synapse}/I_{axon}$ ratio: 3.8 ± 0.3, $n = 15$, $p < 0.001$), whereas the second showed almost normal synaptic targeting ($I_{synapse}/I_{axon}$ ratio: 8.8 ± 1.0, $n = 15$, $p = 0.77$) (supplemental Fig. S1*C*,*D*, available at www.jneurosci.org as supplemental material), an observation consistent with a previous report that the SH3-binding domain mutation of $Ca_v2.2$ reduced synaptic targeting in only 41% of the transfected neurons (Maximov and Bezprozvanny, 2002). Altogether, these results support a notion that although LC2, CASK and MINT are all necessary for synaptic localization of $Ca_v2.2$, LC2 may play a more profound role in anchoring the channels at the presynaptic plasma membrane through its unique mechanism.

$Ca_v2.2$-LC2 interaction is important for presynaptic surface retention of $Ca_v2.2$

To detect surface-expressed endogenous $Ca_v2.2$, we generated a polyclonal anti-$Ca_v2.2$ex antibody against the extracellular loop between IIIS1 and IIIS2 of $Ca_v2.2$. Specificity of this antibody was confirmed by testing its ability to detect the same long (~250 kDa) and short (~140 kDa) $Ca_v2.2$ isoforms in rat brain homogenate (Fig. 4*A*) that were detected with an anti-$Ca_v2.2$in antibody against the intracellular synprint region (Leenders et al., 2002). As a control, detection of $Ca_v2.2$ proteins with the anti-$Ca_v2.2$ex antibody was effectively blocked by preincubation of the antiserum with the IIIS1-IIIS2 peptide. Furthermore, immunoblotting and immunostaining analysis showed that anti-$Ca_v2.2$ex specifically recognized GFP-$Ca_v2.2$ but not GFP-$Ca_v2.1$ expressed in COS-7 cells (supplemental Fig. S2*A*,*B*, available at www.jneurosci.org as supplemental material). Using the anti-$Ca_v2.2$ex antibody, we immunostained fixed but unpermeabilized hippocampal neurons followed by permeabilization and secondary staining with an anti-synaptophysin antibody. Fine punctate staining of the surface $Ca_v2.2$ ($Ca_v2.2$s) was observed along the processes and was completely abolished when the antibody was preincubated with the IIIS1-IIIS2 peptide (Fig. 4*B*). The detected surface $Ca_v2.2$s predominantly colocalized with synaptophysin puncta along the neuronal processes (Fig. 4*B*', white arrows). To exclude the possibility that the fixation process may cause permeabilization, we performed costaining with synaptophysin and $Ca_v2.2$(ex) antibodies. In our nonpermeabilized neurons, there is almost no synaptophysin signal detected, whereas $Ca_v2.2$ surface staining is significantly labeled, indicating very little, if any, permeabilization under our staining conditions (supplemental Fig. S2*C*, available at www.jneurosci.org as supplemental material).

To further investigate the physiological role of the $Ca_v2.2$-LC2 interaction, we sought to analyze the synaptic distribution of endogenous $Ca_v2.2$s using the anti-$Ca_v2.2$ex antibody after expression of the dominant negative binding-domain transgene BD. In the GFP-transfected control neurons, almost all (99.5 ± 0.5%) of the synaptophysin puncta showed detectable surface $Ca_v2.2$ staining (Fig. 4*C*), which was slightly but significantly reduced in neurons expressing BD (87.9 ± 4%, $n = 10$, $p = 0.01$). In addition, expression of BD reduced the normalized mean intensity of $Ca_v2.2$s at synapses by 25% (0.74 ± 0.04, $n = 10$, $p < 0.001$) relative to that from untransfected neurons within the same image (Fig. 4*D*). In contrast, expression of BD showed no significant effect on the fluorescent mean intensity of total synaptic $Ca_v2.2$ detected in permeabilized neurons (supplemental Fig. S3, available at www.jneurosci.org as supplemental material). Expression of BD also had no significant effect on both the puncta density and mean intensity of presynaptic proteins including synaptophysin (Fig. 4*D*), CASK and Bassoon (supplemental Fig. S4, available at www.jneurosci.org as supplemental material), suggesting a selective role for BD in surface retention of the $Ca_v2.2$ channels at presynaptic boutons.

To confirm our findings, we alternatively suppressed LC2 expression with siRNA as a complementary approach. Three MAP1A-HC or LC2-targeted siRNAs and one scrambled control siRNA not homologous to any sequence in GenBank were generated and tested extensively. Both MAP1A HC-targeted siRNA1 and LC2-targeted siRNA3 efficiently reduced endogenously expressed LC2 in the soma of hippocampal neurons by ~50% 5–7 d after transfection (Fig. 5*A*,*C*). In addition, siRNA1 reduced LC2 staining intensity at synaptic sites by ~50% compared with untransfected neurons from the same image or to neurons expressing control siRNA (Fig. 5*B*,*D*). The morphology of neurons and β-tubulin staining showed no significant change after knocking down LC2 expression (Fig. 5*A*). In contrast, a 25% reduction was found in the normalized fluorescent mean intensity of the synaptic surface $Ca_v2.2$s after transfection with siRNA1 (0.76 ± 0.07, $n = 15$) relative to those expressing the control siRNA (1.02 ± 0.03, $n = 16$, $p < 0.001$) (Fig. 5*E*,*F*). The siRNA1 was designed to target a sequence in the coding region for MAP1A-HC (nt3827–3847), thus selectively suppressing HC and consequently LC2, which is generated by proteolytic cleavage from HC. Therefore, exogenous expression of HA-LC2 was resistant to siRNA1 (supplemental Fig. S5, available at www.jneurosci.org as supplemental material), providing a rescue approach by coexpressing siRNA1 and HA-LC2 in neurons. Cotransfection of HA-LC2 with siRNA1 efficiently rescued the RNAi phenotype of the reduced surface intensity of $Ca_v2.2$s (Fig. 5*E*,*F*). However, cotransfection of HA-LC2NT, the N-terminal half of LC2 capable of binding $Ca_v2.2$, was unable to rescue the RNAi phenotype, indicating that the surface anchoring of $Ca_v2.2$ at synapses required proper expression of the full-length LC2 in neurons.

Interference of the LC2–$Ca_v2.2$ interaction leads to reduced Ca^{2+}-transients at presynaptic boutons

Presynaptic Ca^{2+} channels mediate the depolarization-induced Ca^{2+} influx into nerve terminals, which triggers synaptic vesicle exocytosis. Defective surface retention of $Ca_v2.2$ might reduce Ca^{2+} transients at presynaptic boutons. The small size of the terminals in cultured hippocampal neurons prevented using electrodes to record presynaptic Ca^{2+} currents. To test our hypothesis, we alternatively conducted calcium imaging at nerve

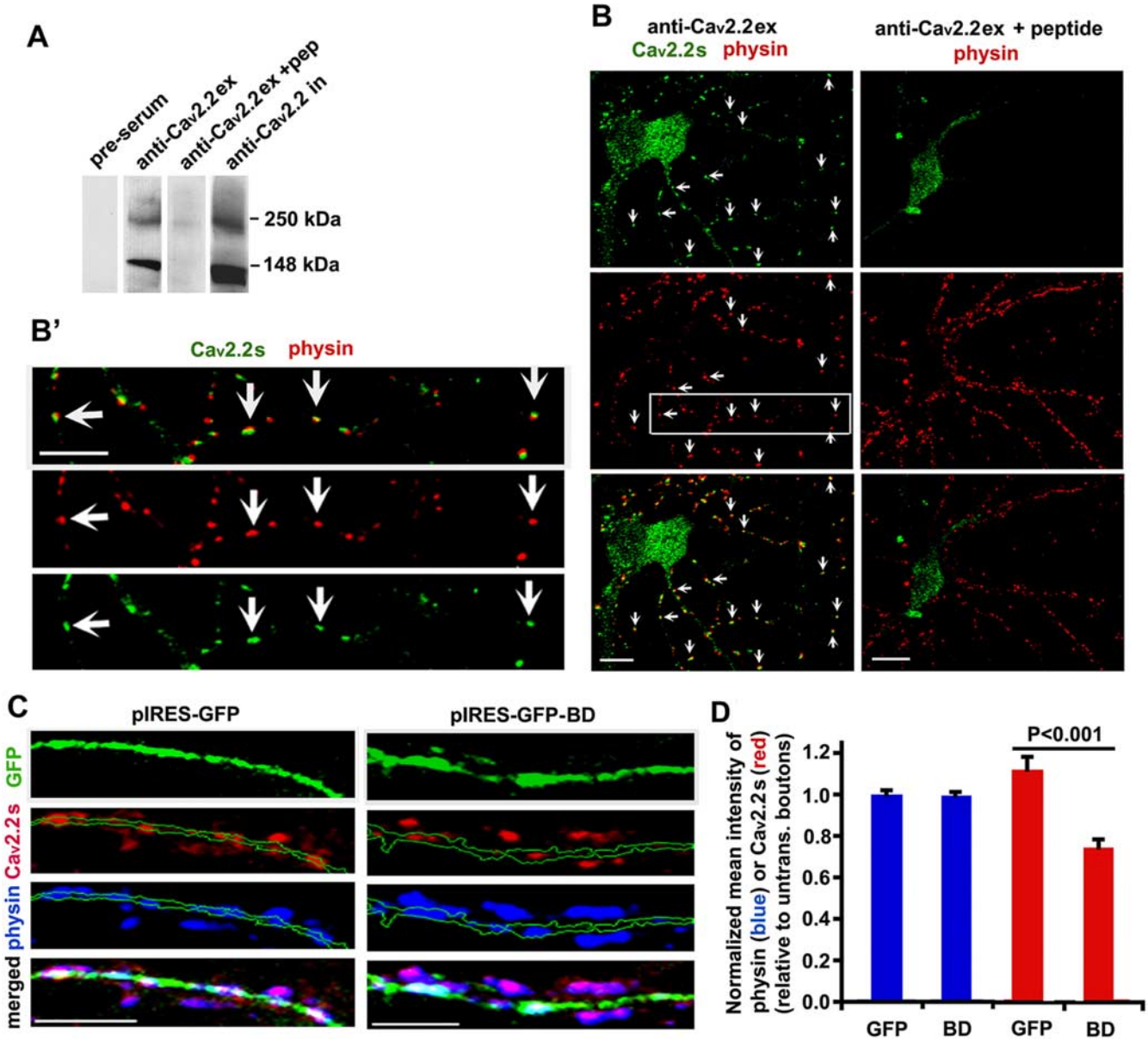

Figure 4. Expression of BD decreased presynaptic surface density of endogenous $Ca_v2.2$. ***A***, Detection of $\alpha 1$ subunit of $Ca_v2.2$ in rat brain homogenates. Anti-$Ca_v2.2$ex (against the extracellular loop between IIIS1–S2) and anti-$Ca_v2.2$in (against the intracellular synprint region between II–III) antibodies detected both ~250 and ~140 kDa bands of $Ca_v2.2$. No signal was detected after preincubation of anti-$Ca_v2.2$ex with the IIIS1–S2 peptide (pep). ***B***, Representative images of cultured hippocampal neurons (19 DIV) coimmunostained with anti-$Ca_v2.2$ex (green) and anti-synaptophysin (red) antibodies. Immunostaining with anti-$Ca_v2.2$ex antibody was performed on fixed nonpermeabilized neurons to detect surface $Ca_v2.2$s, followed by permeabilization and second staining for synaptophysin. Colocalization of the two proteins is indicated by arrow. Surface staining of $Ca_v2.2$s at synapses was abolished when the anti-$Ca_v2.2$ex antibody was preincubated with the IIIS1-S2 peptide. ***B'***, Close-up views of the boxed region in ***B***. ***C***, Representative images of axonal segments of hippocampal neurons transfected with pIRES-EGFP vector or pIRES-EGFP-BD at 9 DIV and coimmunostained for surface $Ca_v2.2$s (red) and synaptophysin (blue) at 14 DIV. Note that the synaptophysin puncta outside the green boundaries are from nontransfected neurons. ***D***, Expression of BD resulted in a reduced mean fluorescent intensity of the surface $Ca_v2.2$ s at presynaptic boutons. Data are means ± SEM; 240 synaptic puncta pooled from 10 neurons in three separate neuronal cultures were measured for each condition. Scale bars, 10 μm.

terminals using Fluo-4 NW. The interaction of LC2–$Ca_v2.2$ was interrupted by expressing the dominant-negative transgene BD at 7 DIV, whereas presynaptic boutons were labeled with DsRed-synaptophysin (Fig. 6*A*). Because of the relatively low signal-to-noise ratio of calcium transients at individual boutons in response to a single stimulation, we applied train stimulation (30 pulses at 10 Hz). At 13–15 DIV, calcium signal within the bouton was imaged every 50 ms for a total of 15 s. The change in fluorescence intensity of Fluo-4 NW over baseline ($\Delta F/F_0$) at presynaptic boutons showed an initial fast-rising phase immediately after stimulation, followed by a relatively slow-rising phase, and finally a rapid recovery after stimulation (Fig. 6*B*). Baseline fluorescence (F_0) was calculated from the first 2 s of images before the field stimulation was applied; individual time points are expressed as percentage increase in fluorescence intensity value over baseline ($\Delta F/F_0$). Peak values of $\Delta F/F_0$ averaged from the last 10 stimuli (20 frames of calcium imaging) were significantly smaller in neurons expressing BD (56.63 ± 3.39%, $n = 116$) than those found in control neurons (83.96 ± 3.55%, $n = 123$, $p < 0.001$).

Ca^{2+} entering through both $Ca_v2.1$ and $Ca_v2.2$ channels is responsible for initiating synaptic transmission at most central synapses (Dunlap et al., 1995). To establish the relative contribu-

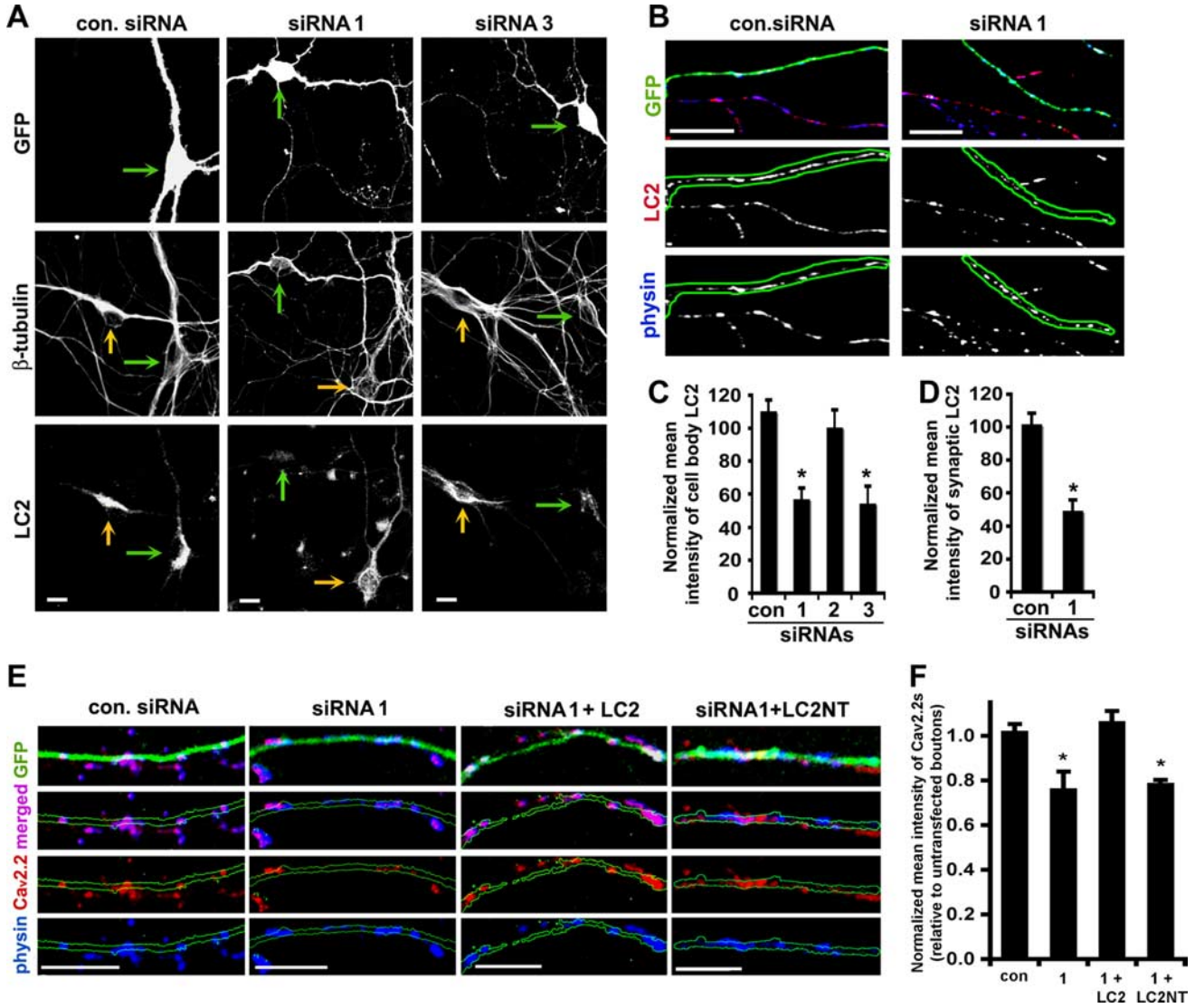

Figure 5. siRNA knock-down of LC2 decreased the synaptic surface density of $Ca_v2.2$. ***A***, Representative images of cultured hippocampal neurons transfected with control siRNA, LC2 siRNA1 (nt3827–3847), or siRNA3 (nt8746 – 8766) at 7 DIV followed by immunostaining at 14 DIV. Expression of the LC2 siRNAs significantly reduced the staining intensity of LC2 (green arrows) compared with untransfected neurons (yellow arrows). ***B***, Representative images of axon segments from siRNA-transfected (green) and untransfected neurons immunostained for LC2 and synaptophysin. ***C***, ***D***, Mean fluorescent intensities of LC2 in cell bodies (***C***) and at presynaptic boutons (***D***) in the transfected neurons normalized to that of nontransfected neurons in the same image. Data are means ± SEM; $n = 12$ from three experiments. ***E***, Representative images of axonal segments of hippocampal neurons transfected with indicated siRNA or for rescue by coexpressing HA-LC2 or HA-LC2NT at 7DIV, and coimmunostained at 14DIV for the surface $Ca_v2.2$s (red) and synaptophysin (blue). ***F***, Mean intensity of surface $Ca_v2.2$s staining at boutons from the transfected neurons was normalized to the mean intensity from untransfected neurons in the same image. Data are means ± SEM of >300 puncta pooled from 15 (siRNA1), 16 (control siRNA), 10 (siRNA+HA-LC2), and 15 (siRNA+HA-LC2NT) neurons in three cultures. (*$p < 0.01$ by Student's *t* test). Scale bars, 10 μm.

tions made by these two channel types in our cultured neurons, we compared Ca^{2+}-influx into presynaptic boutons before and 10 min after applying selective channel blockers: ω-agatoxin IVA (ω-Aga) (100 nM) for $Ca_v2.1$ and ω-conotoxin GVIA (ω-CgTx) (1 μM) for $Ca_v2.2$. Application of either toxin significantly reduced the Ca^{2+}-transients at nerve terminals (Fig. 6*C*; supplemental Table 1, available at www.jneurosci.org as supplemental material). ω-Aga reduced the peak $\Delta F/F_0$ by 26.21 ± 4.76%; however, ω-CgTx reduced the peak $\Delta F/F_0$ to a much greater extent (62.05 ± 3.11%) (Fig. 6*E*). These results suggest that relative to $Ca_v2.1$, $Ca_v2.2$ primarily contributed to total Ca^{2+}-influx at presynaptic boutons of 2-week-old hippocampal neurons, which agrees with previous observations from the same preparations (Scholz and Miller, 1995). To test whether BD affected Ca^{2+}-transients selectively through $Ca_v2.2$ channels, we applied the toxins to the BD-transfected neurons (Fig. 6*D*,*E*). In these neurons, application of ω-Aga reduced the peak $\Delta F/F_0$ to 35.93 ± 2.35%, a further reduction of ~50% relative to the peak $\Delta F/F_0$ observed in the control GFP-transfected boutons ($p < 0.001$). In contrast, blocking $Ca_v2.2$ with ω-CgTx only slightly reduced the peak $\Delta F/F_0$ in neurons expressing BD (31.16 ± 3.64%), compared with that of control neurons (37.95 ± 3.11%, $p = 0.2$). The less inhibitory effect of ω-CgTx and larger inhibitory effect of ω-Aga on neurons expressing BD than that in control neurons suggest that BD selectively reduced Ca^{2+}-influx into presynaptic boutons through $Ca_v2.2$ channels.

LC2 knockdown reduces the density of active presynaptic boutons

We next examined whether the reduced Ca^{2+}-influx impaired functional release sites by analyzing uptake and recycling of the styryl dye FM4-64 in cultured hippocampal neurons after LC2

knockdown. Neurons were transfected with siRNAs at 7 DIV; FM4-64 measurements were performed at 13–15 DIV. FM4-64 dye was taken up in an activity-dependent manner, because the majority of FM4-64 at synaptic terminals was unloaded by 50 mM K^+ stimulation in both control siRNA- and siRNA1-transfected neurons (Fig. 7*A*). However, LC2 knockdown significantly decreased the density of FM4-64 puncta (2.3 ± 0.2 per 10 μm) compared with that in neurons expressing control siRNA (3.1 ± 0.1 per 10 μm, $p < 0.01$) (Fig. 7*B*) or untransfected neurons (3.5 ± 0.3 per 10 μm, $p < 0.01$). The reduced FM4-64 uptake is unlikely attributed to impaired assembly of presynaptic boutons because the density of synaptophysin puncta along axonal processes was unaffected after siRNA1 transfection (Fig. 7*B*).

Next, we sought to determine whether the defect in presynaptic activity was attributable to reduced Ca^{2+}-influx through $Ca_v2.2$ channels by comparing FM4-64 loading before and after applying $Ca_v2.2$ or $Ca_v2.1$ selective blockers. Neurons were imaged after a 2 min high K^+-stimulated loading (L1) of FM4-64 to assess active release sites. After extended washing and unloading, neurons were incubated for 10 min with either ω-CgTx (1 μM) or ω-Aga (100 nM) followed by a second 2 min high K^+-induced FM4-64 loading (L2) (Fig. 7*C*). In the absence of any toxin, nearly all FM4-64 puncta (89.3 ± 1.2%) observed at L1 were also detected at L2 (supplemental Table 2, available at www.jneurosci.org as supplemental material). Therefore, by evaluating the difference between L1 and L2 from the same image fields, we assessed the relative inhibition of presynaptic activity by the toxins. Both toxins significantly lowered the density of FM4-64-labeled boutons in untransfected neurons, with a slightly larger reduction caused by ω-CgTx (32.5 ± 2.1%, $n = 944$) than ω-Aga (38.1 ± 3.5%) (Figs. 7*D*,*E*). Application of ω-CgTx reduced the density of active boutons in the siRNA1-transfected neurons to a level (31.1 ± 2.8%, $n = 406$) similar to that in the untransfected controls (32.5 ± 2.1%, $p = 0.7$). In contrast, ω-Aga had a more profound effect in reducing the density of FM4-64 puncta in neurons expressing siRNA1 (30.5 ± 3.2%, $n = 693$) compared with that in untransfected neurons (38.1 ± 3.5%, $p < 0.05$). FM4-64 measurements were consistent with our observations from the Ca^{2+}-transient analysis and further suggested that presynaptic activity depended on the proper surface expression of both $Ca_v2.2$ and $Ca_v2.1$ channels.

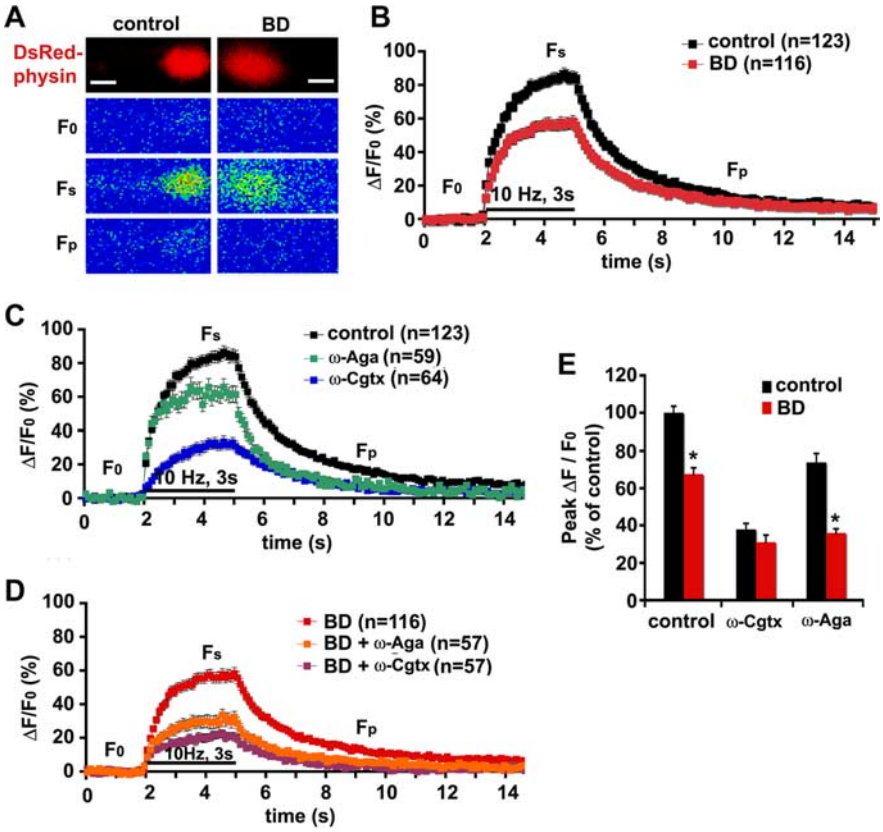

Figure 6. Expression of BD reduced Ca^{2+}-transients at presynaptic boutons. ***A***, Representative calcium transients at presynaptic boutons of neurons cotransfected at 7–9 DIV with DsRed-monomer-synaptophysin (DsRed-physin) and HA-BD or HA (control). Three representative images of boutons showing Fluo-4 NW signal before (F_0), at the end of (F_s), and after stimulation (F_p). Images are pseudocolored, with blue representing low [Ca^{2+}] concentration and red representing high [Ca^{2+}] concentration, Scale bars, 1 μm. ***B***, Time course of changes in Fluo-4 NW fluorescent intensity over baseline ($\Delta F/F_0$) from the presynaptic boutons of the neurons expressing control HA (black trace) or HA-BD (red trace). ***C***, ***D***, Time course of changes in fluorescence intensity over baseline ($\Delta F/F_0$) before and after application of ω-Aga (100 nM) or ω-Cgtx (1 μM) in the boutons from neurons expressing control HA (***C***) or HA-BD (***D***). ***E***, Averaged peak $\Delta F/F_0$ values from traces shown in ***C*** and ***D*** during field stimulation (F_s) and expressed as percentage of the peak $\Delta F/F_0$ values in control boutons. (*$p < 0.01$ by Student's *t* test).

The actin cytoskeleton is important for surface expression of $Ca_v2.2$

LC2 associates with both the actin and MT cytoskeleton (Noiges et al., 2002). One candidate function of the LC2-$Ca_v2.2$ interaction is to anchor the channel to the presynaptically enriched actin-cytoskeleton, thereby retaining the channel at the plasma membrane of nerve terminals. To test this hypothesis, we treated hippocampal neurons for 1 h with Latrunculin A (LAT) (2.5 μM) to disrupt actin filaments or with Nocodazole (NOC) (5 μM) to disassemble MT, followed by coimmunostaining for synaptophysin, Bassoon and surface $Ca_v2.2$s and total $Ca_v2.2$t (Figs. 8*A*–*C*). Treatment with these reagents substantially reduced the staining of phalloidin (for actin) or β-tubulin (for MT) when compared with control neurons treated with DMSO control (supplemental Fig. S6, available at www.jneurosci.org as supplemental material) without changing overall staining patterns of synaptophysin and Bassoon (Fig. 8*C*). However, treating neurons with LAT but with neither NOC nor DMSO selectively reduced the density of surface $Ca_v2.2$s-positive boutons by 44.2 ± 8.6% ($p < 0.001$) (Fig. 8*D*) and fluorescent mean intensity of the surface $Ca_v2.2$s in the remaining boutons by 41.2 ± 6.8% ($p < 0.001$) (Fig. 8*E*). Furthermore, disruption of actin filaments did not affect the distribution of total $Ca_v2.2$t at nerve terminals (Fig. 8*B*,*D*,*E*). In light of the correlated reduction in surface $Ca_v2.2$ and calcium transients at nerve terminals by either interfering with the LC2–$Ca_v2.2$ coupling or by disrupting actin filaments, a simple cellular explanation for our observations is that LC2-mediated retention of the presynaptic surface $Ca_v2.2$ is likely occurred through an actin-based anchoring mechanism.

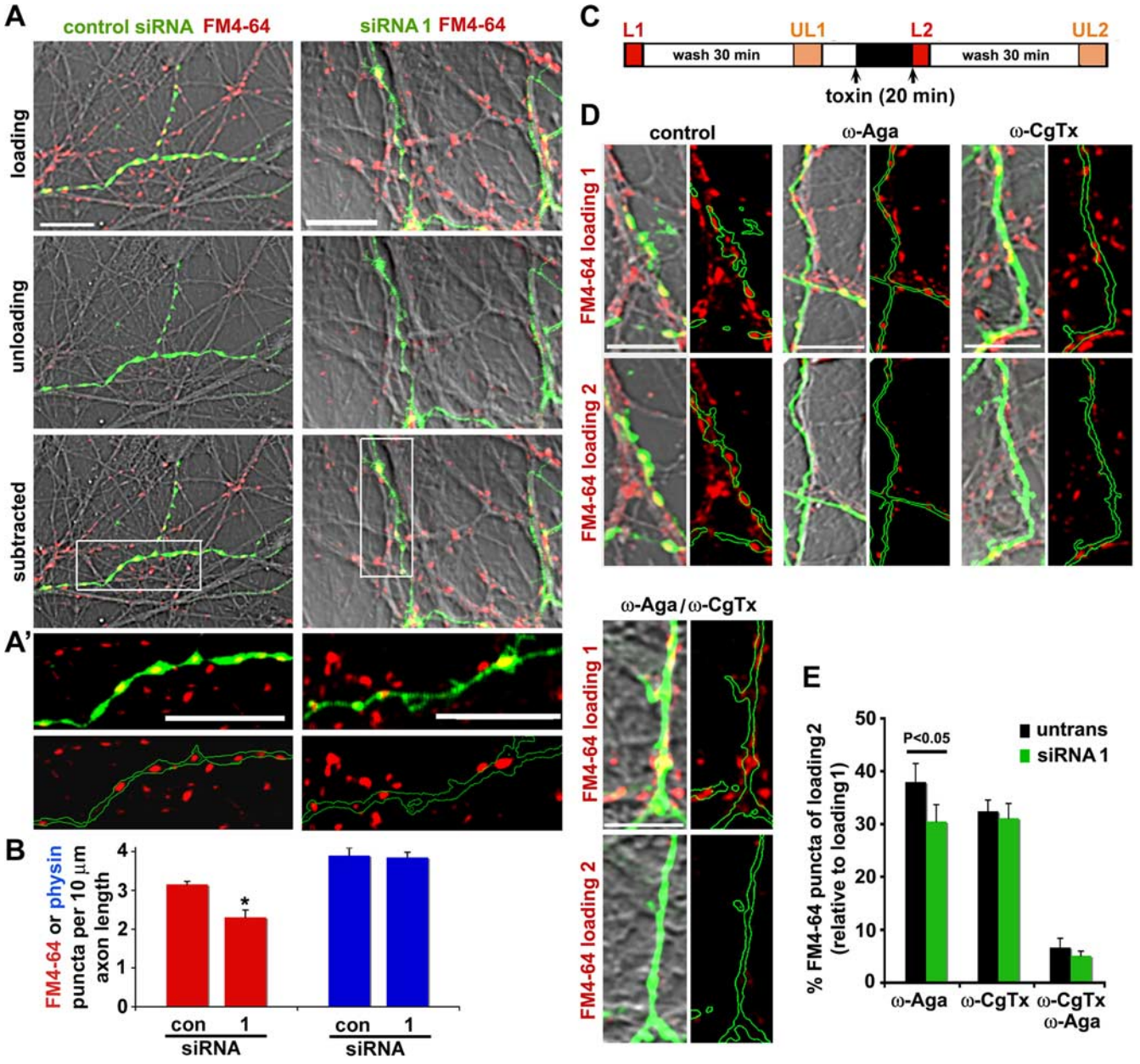

Figure 7. Suppressing LC2 expression reduced the density of FM4-64-labeled active synapses. ***A***, Representative images showing activity-dependent loading and unloading of FM4-64 dye at presynaptic boutons of hippocampal neurons transfected with control siRNA or siRNA1. Neurons were loaded with FM4-64 dye in high K^+ (50 mM) solution for 2 min (loading), washed in Tyrode solution for 30 min, then unloaded by high K^+ perfusion for 5 min (unloading). Activity-dependent uptake of FM4-64 at synapses was represented by subtracting unloading signals from the loading image (subtracted). ***A'***, Close-up views of the boxed region in ***A***. GFP (green) marks transfected neurons. ***B***, Quantitative analysis showing reduced density of FM4-64 uptake along axonal processes after knocking down LC2 expression (control: 3.1 ± 0.1; siRNA1: 2.3 ± 0.2, $p < 0.01$). siRNA1 had no effect on the density of synaptophysin-labeled boutons (control: 4.0 ± 0.2; siRNA1: 4.1 ± 0.2, $p = 0.64$). Total axon length measured for FM4-64 puncta: 7608 μm (con siRNA) and 7912 μm (siRNA1); for synaptophysin puncta: 1223 μm (con siRNA) and 1071 μm (siRNA1). ***C***, Experimental protocol for FM4-64 loading (L) and unloading (UL) before and after toxin applications. ***D***, Representative images of activity-dependent FM4-64 uptake before (loading 1) and after (loading 2) application (10 min) of ω-Aga (100 nM), or ω-CgTx (1 μM), or both toxins. ***E***, Percentage of FM4-64 puncta after toxin application (loading 2) relative to that before toxin application (loading 1). Data are means ± SEM from >400 FM4-64 puncta for each condition and pooled from 12 neurons from three experiments. Scale bars, 10 μm.

Discussion

In this study, we reveal that the surface density of the $Ca_v2.2$ channels at synapses is regulated through its interaction with LC2. Using an antibody against an extracellular epitope of $Ca_v2.2$ and measurements of calcium transients and synaptic activity in live neurons combined with expression of the binding domain transgene and siRNA, we provide molecular and cellular evidence that the $Ca_v2.2$-LC2 interaction is critical for maintaining $Ca_v2.2$ surface density and thus, proper synapse function.

Although previous studies showed that CASK, MINT and dynein motor light chain TcTex1 are important for synaptic targeting of $Ca_v2.2$ (Maximov and Bezprozvanny, 2002; Lai et al., 2005), our current study indicates that LC2 acts as an important protein for anchoring $Ca_v2.2$ at presynaptic surfaces. This newly identified interaction involved a short binding sequence located upstream of the SH3 (for CASK binding) and PDZ (for Mint binding) binding domains within the $Ca_v2.2$ C terminus. We found that deleting the LC2-binding domain had no effect on the interaction of $Ca_v2.2$ with CASK and Mint1 (supplemental Fig. S1, available at www.jneurosci.org as supplemental material). In

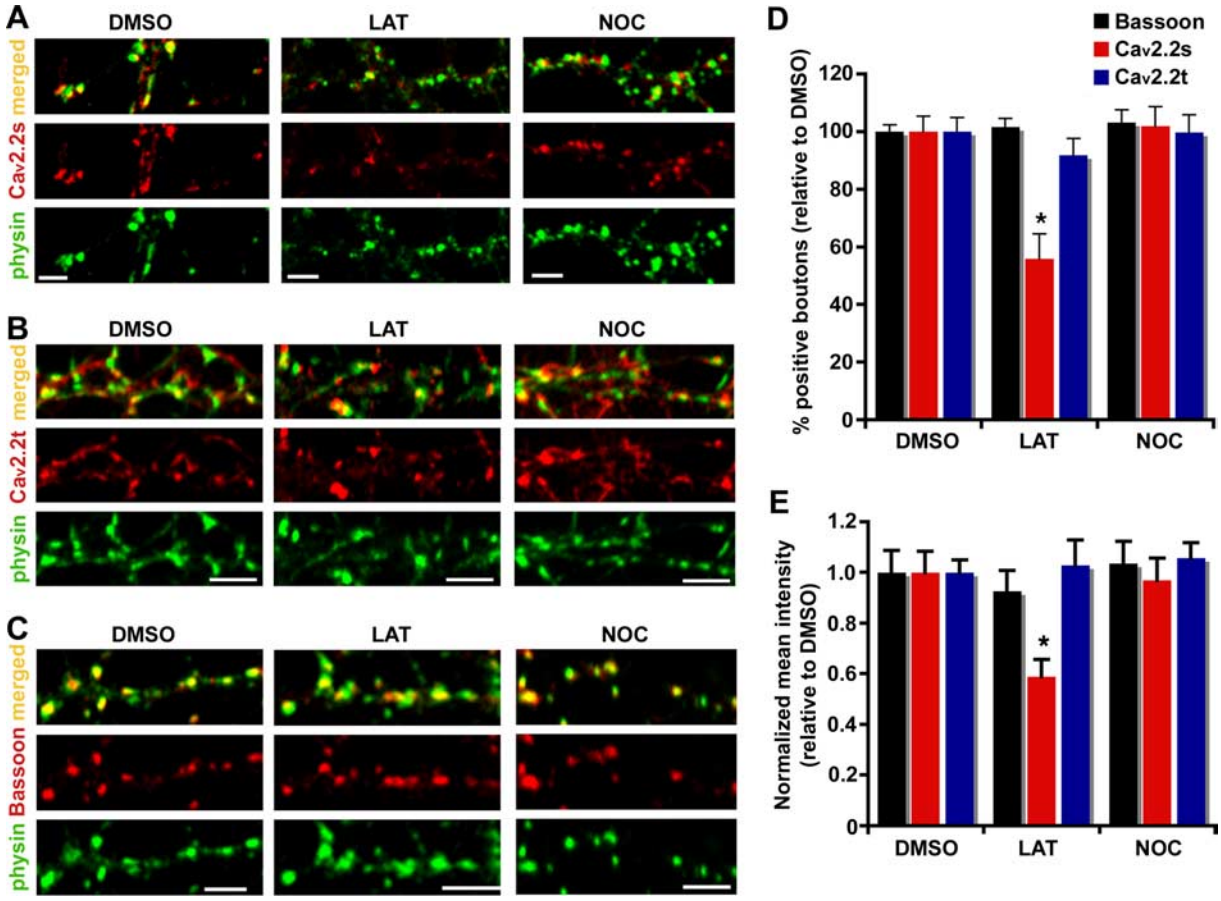

Figure 8. Disruption of the actin cytoskeleton reduced synaptic $Ca_v2.2$ surface density. ***A–C***, Representative images of axonal segments of hippocampal neurons treated for 1 h at 37°C with DMSO, LAT (2.5 μM) or NOC (5 μM) and coimmunostained for synaptophysin (green) and surface $Ca_v2.2$s (red; ***A***), or total $Ca_v2.2$t (red; ***B***), or Bassoon (red; ***C***). ***D***, ***E***, Quantifications of $Ca_v2.2$s (red bars), Cav2.2t (blue bars) and Bassoon (black bars) signal at synaptophysin-labeled boutons. Percentage of positive boutons (***D***) and normalized mean fluorescent intensity (***E***) were analyzed for each treatment from over 600 boutons from at least 15 neurons collected from three experiments (*$p < 0.001$ by Student's *t* test). Scale bars, 10 μm.

addition, no interaction was detectable between BD and TcTex1 (data not shown). Furthermore, whereas the sequences of the binding domains for CASK and Mint were conserved between $Ca_v2.2$ and $Ca_v2.1$, the LC2-binding domain was specific for $Ca_v2.2$ (Fig. 1*F*). Thus, our observations showing the reduced surface expression and calcium transients at presynaptic boutons and impaired FM dye uptake were likely specific for disrupting LC2–$Ca_v2.2$ coupling. It is conceivable that both $Ca_v2.1$ and $Ca_v2.2$ channels were transported and targeted to presynaptic terminals through a similar mechanism, whereas the final surface retention was likely mediated by a channel-specific interaction with cytoskeleton-associated proteins. The latter agrees with the "channel type preferring slots" as proposed by Cao et al. (2004).

To investigate the specific role of LC2 in $Ca_v2.2$ presynaptic surface retention, we used a 23-residue LC2-BD as a dominant-negative transgene or expressed the $Ca_v2.2$ mutant lacking BD, instead of expressing a long $Ca_v2.2$ C-terminal sequence containing multiple structural determinants as in previous studies (Maximov and Bezprozvanny, 2002; Lai et al., 2005). In addition, application of an antibody against the extracellular loop of $Ca_v2.2$ in unpermeabilized neurons allowed us to distinguish surface localization from synaptic targeting of the $Ca_v2.2$ channels and provided more direct evidence for a unique role of LC2 in retaining $Ca_v2.2$ at the presynaptic plasma membrane. It is unlikely that LC2 is primarily involved in controlling mobility of $Ca_v2.2$ along the plasma membrane based on our following observations in the neurons expressing either BD or siRNA: (1) the surface staining did not reveal dispersion of $Ca_v2.2$ outside the terminals, and (2) intrasynaptic staining in the permeabilized neurons showed that $Ca_v2.2$ signal was retained within the terminals (supplemental Fig. S3C, available at www.jneurosci.org as supplemental material). Thus, our observations consistently favor the possibility that disruption of LC2–$Ca_v2.2$ coupling would result in the recruitment of the endogenous $Ca_v2.2$ from the surface into the intrasynaptic pool. One possible explanation for GFP–$Ca_v2.2$ dispersion into axons might be attributed to over saturation of this pool by excess channels, leading to "overflow" of GFP–$Ca_v2.2$ into the axon. Altogether, these findings support a complex mechanical model in which different structural domains within the $Ca_v2.2$ C terminus coordinately regulate their axonal trafficking, synaptic targeting, and surface localization, likely through multiple interactions with motor proteins, active zone scaffold proteins, and cytoskeleton-associated proteins. It will be important in the future to address how all the various motifs coordinate their activities to determine the final synaptic location of $Ca_v2.2$ and how this complex mechanism is modulated developmentally and regulated in response to synaptic activity.

Expression of the BD transgene and suppressing LC2 with RNAi had no effect on the density of the synaptic vesicle protein synaptophysin, active zone cytomatrix protein Bassoon and scaffold protein CASK, thus, excluded a nonspecific effect on synaptic integrity. Our findings for the partial inhibitory effects on

Ca^{2+} transients and FM4-64 uptake were consistent with results from previous observations that presynaptic activity is controlled by multiple calcium channels at most central synapses (Dunlap et al., 1995; Wu and Saggau, 1997). Relative to $Ca_v2.1$, $Ca_v2.2$ primarily contributed to total Ca^{2+}-influx into presynaptic boutons of our rat hippocampal neurons at 12–15 DIV. These findings agreed with previous observations at developing synapses of hippocampal neurons (10–15 DIV), in which ω-CgTx GVIA blocked transmission by >80%, whereas ω-Aga IVA was less effective (Scholz and Miller, 1995). A previous study using FM1-43 imaging in hippocampal neurons showed that ~45% of synapses rely solely on the ω-CgTx GVIA-sensitive N-type calcium channels and the remaining synapses were supported by both N- and P/Q-type calcium channels (Reuter, 1995). Our study demonstrated that interference of the LC2-$Ca_v2.2$ interaction combined with application of ω-Aga IVA, but not with ω-CgTx GVIA, resulted in additional reduction in both activity-dependent Ca^{2+}-influx and FM dye uptake. Thus, it is likely that those observed phenotypes were attributable to reduced Ca^{2+} influx into nerve terminals selectively through the $Ca_v2.2$ but not $Ca_v2.1$ channels, resulting in presynaptic $[Ca^{2+}]$ below the threshold levels for triggering synaptic vesicle exocytosis in a small fraction of the synapses. Although reduced Ca^{2+}-influx is consistent with the observed reduction in surface density of $Ca_v2.2$ after disrupting the LC2-$Ca_v2.2$ interaction, regulation of $Ca_v2.2$ channel gating by LC2 cannot be completely excluded.

LC2 is a proteolytic product of the MAP1A gene and generated via a post-translational cleavage from the MAP1A heavy chain (Langkopf et al., 1992). Using an anti-LC2 antibody, our analysis at light and electron microscopic levels clearly demonstrated a synaptic localization of LC2 although it also distributes within soma and along neuronal processes. In contrast, less significant staining of MAP1A-HC was detected at synapses from hippocampal neurons. Our biochemical analysis of synaptosomal fractionation further suggests that LC2, but not MAP1A-HC, was present in the membrane-enriched fraction at nerve terminals, probably through its interactions with the membrane-anchored channels and receptors. Furthermore, exogenously expressed LC2 rescued the surface localization of $Ca_v2.2$ when expression of both endogenous MAP1A-HC and LC2 was suppressed by siRNA, supporting the notion that LC2 itself was sufficient for retaining $Ca_v2.2$ channels at the presynaptic plasma membrane.

Emerging evidence suggests critical roles for various cytoskeleton-associated proteins in the surface expression of ion channels and receptors (for review, see Lai and Jan, 2006). For example, Kir2.1 (Sampson et al., 2003) and $K_v4.2$ (Petrecca et al., 2000) showed markedly decreased levels of functional cell surface expression in the absence of the actin cytoskeleton linker protein filamin. Thus, it is likely that LC2 serves as a linker between $Ca_v2.2$ and the cytomatric actin cytoskeleton within the active zone and structurally stabilizes the channels at the presynaptic plasma membrane. In support of this hypothesis, we showed that disruption of the actin cytoskeleton by Latrunculin A removed $Ca_v2.2$ from the synaptic plasma membrane. The anchoring function of LC2 was further supported by our observations that the LC2 NT half, which can associate with $Ca_v2.2$ but unable to bind actin (Noiges et al., 2002), did not rescue the siRNA phenotype. Although the mechanism remains to be further elucidated, an attractive model is that $Ca_v2.2$–LC2 coupling with presynaptic actin might be essential for local trafficking and anchoring of the channels at the plasma membrane. LC2 may play a role in the targeted insertion of $Ca_v2.2$ into the plasma membrane as proposed for the cytoskeleton-associated protein filamin in recycling G-protein coupled receptors (Seck et al., 2003). Alternatively, LC2 and actin may provide the anchoring platform for $Ca_v2.2$ at nerve terminals and disrupting this coupling consequently resulted in unstable retention or even removal of $Ca_v2.2$ from the plasma membrane, probably via internalization. This hypothesis agrees with the recent report that $Ca_v2.2$ internalization is mediated by G-protein coupled receptors (Altier et al., 2006) and triggered by disrupting the channel-cytoskeleton interaction (Tombler et al., 2006). Moreover, it may account for the specific role for LC2 in $Ca_v2.2$ surface expression, as it is well established that G-protein-mediated inhibition is more effective for $Ca_v2.2$ than $Ca_v2.1$ channels at synapses (Currie and Fox, 1997).

Although our current study made progress in identifying a novel LC2-$Ca_v2.2$ interaction critical for surface expression of the channels at presynaptic terminals, it remains to be tested whether LC2 promotes membrane integration of $Ca_v2.2$ or prevents its internalization. How is LC2-mediated surface anchoring of $Ca_v2.2$ regulated in response to neuronal activity and synaptic modulation? Future studies using genetic mouse models combined with gene rescue experiments will be critical to elucidate mechanisms for synaptic targeting and retention of the $Ca_v2.2$ channels during synaptogenesis and at mature synapses under various physiological conditions.

References

Altier C, Khosravani H, Evans RM, Hameed S, Peloquin JB, Vartian BA, Chen L, Beedle AM, Ferguson SS, Mezghrani A, Dubel SJ, Bourinet E, McRory JE, Zamponi GW (2006) ORL1 receptor–mediated internalization of N-type calcium channels. Nat Neurosci 9:31–40.

Bennett V, Lambert S (1999) Physiological roles of axonal ankyrins in survival of premyelinated axons and localization of voltage-gated sodium channels. J Neurocytol 28:303–318.

Cao YQ, Piedras-Rentería ES, Smith GB, Chen G, Harata NC, Tsien RW (2004) Presynaptic Ca^{2+} channels compete for channel type-preferring slots in altered neurotransmission arising from Ca^{2+} channelopathy. Neuron 43:387–400.

Catterall WA (2000) Structure and regulation of voltage-gated Ca^{2+} channels. Annu Rev Cell Dev Biol 16:521–555.

Craig AM, Banker G (1994) Neuronal polarity. Annu Rev Neurosci 17:267–310.

Currie KP, Fox AP (1997) Comparison of N- and P-type voltage-gated calcium channel inhibition. J Neurosci 17:4570–4579.

Dunlap K, Luebke JI, Turner TJ (1995) Exocytotic Ca^{2+} channels in mammalian central neurons. Trends Neurosci 18:89–98.

Ertel EA, Campbell KP, Harpold MM, Hofmann F, Mori Y, Perez-Reyes E, Schwartz A, Snutch TP, Tanabe T, Birnbaumer L, Tsien RW, Catterall WA (2000) Nomenclature of voltage-gated calcium channels. Neuron 25:533–535.

Goslin K, Asmussen H, Banker G (1998) Rat Hippocampal neurons in low-density culture. In: Culturing nerve cells, Ed 2 (Banker G, Goslin K, eds), pp 339–370. Cambridge, MA: MIT.

Hammarback JA, Obar RA, Hughes SM, Vallee RB (1991) MAP1B is encoded as a polyprotein that is processed to form a complex N-terminal microtubule-binding domain. Neuron 7:129–139.

Hattan D, Nesti E, Cachero TG, Morielli AD (2002) Tyrosine phosphorylation of Kv1.2 modulates its interaction with the actin-binding protein cortactin. J Biol Chem 277:38596–38606.

Ilardi JM, Mochida S, Sheng ZH (1999) Snapin a SNARE-associated protein implicated in synaptic transmission. Nat Neurosci 2:119–124.

Ives JH, Fung S, Tiwari P, Payne HL, Thompson CL (2004) Microtubule-associated protein light chain 2 is a stargazin-AMPA receptor complex-interacting protein in vivo. J Biol Chem 279:31002–31009.

Khanna R, Sun L, Li Q, Guo L, Stanley EF (2006) Long splice variant N type calcium channels are clustered at presynaptic transmitter release sites without modular adaptor proteins. Neuroscience 138:1115–1125.

Lai HC, Jan LY (2006) The distribution and targeting of neuronal voltage-gated ion channels. Nat Rev Neurosci 7:548–562.

Lai M, Wang F, Rohan JG, Maeno-Hikichi Y, Chen Y, Zhou Y, Gao G, Sather

WA, Zhang JF (2005) A tctex1-Ca^{2+} channel complex for selective surface expression of Ca^{2+} channels in neurons. Nat Neurosci 8:435–442.

Langkopf A, Hammarback JA, Müller R, Vallee RB, Garner CC (1992) Microtubule-associated proteins 1A and LC2. Two proteins encoded in one messenger RNA. J Biol Chem 267:16561–16566.

Lao G, Scheuss V, Gerwin CM, Su Q, Mochida S, Rettig J, Sheng ZH (2000) Syntaphilin: a syntaxin-1 clamp that controls SNARE assembly. Neuron 25:191–201.

Leenders AG, van den Maagdenberg AM, Lopes da Silva FH, Sheng ZH, Molenaar PC, Ghijsen WE (2002) Neurotransmitter release from tottering mice nerve terminals with reduced expression of mutated P-, Q-type Ca^{2+}-channels. Eur J Neurosci 15:13–18.

Leenders M, Gerwin C, Sheng ZH (2004) Multidisciplinary approaches for characterizing synaptic vesicle proteins. In: Current protocols in neuroscience (Taylor G, ed), pp Unit 2.7: 2.7.1–2.7.18. Hoboken, NJ: Wiley.

Lisman JE, Raghavachari S, Tsien RW (2007) The sequence of events that underlie quantal transmission at central glutamatergic synapses. Nat Rev Neurosci 8:597–609.

Maruoka ND, Steele DF, Au BP, Dan P, Zhang X, Moore ED, Fedida D (2000) Alpha-actinin-2 couples to cardiac Kv1.5 channels, regulating current density and channel localization in HEK cells. FEBS Lett 473:188–194.

Matus A (1988) Microtubule-associated proteins: their potential role in determining neuronal morphology. Annu Rev Neurosci 11:29–44.

Maurer MH, Grünewald S, Gassler N, Rossner M, Propst F, Würz R, Weber D, Kuner T, Kuschinsky W, Schneider A (2004) Cloning of a novel neuronally expressed orphan G-protein-coupled receptor which is upregulated by erythropoietin, interacts with microtubule-associated protein 1b and colocalizes with the 5-hydroxytryptamine 2a receptor. J Neurochem 91:1007–1017.

Maximov A, Bezprozvanny I (2002) Synaptic targeting of N-type calcium channels in hippocampal neurons. J Neurosci 22:6939–6952.

Mochida S, Westenbroek RE, Yokoyama CT, Zhong H, Myers SJ, Scheuer T, Itoh K, Catterall WA (2003) Requirement for the synaptic protein interaction site for reconstitution of synaptic transmission by P/Q-type calcium channels. Proc Natl Acad Sci U S A 100:2819–2824.

Noiges R, Eichinger R, Kutschera W, Fischer I, Nemeth Z, Wiche G, Propst F (2002) Microtubule-associated protein 1A (MAP1A) and MAP1B: light chains determine distinct functional properties. J Neurosci 22:2106–2114.

Park SM, Liu G, Kubal A, Fury M, Cao L, Marx SO (2004) Direct interaction between BKCa potassium channel and microtubule-associated protein 1A. FEBS Lett 570:143–148.

Petrecca K, Miller DM, Shrier A (2000) Localization and enhanced current density of the Kv4.2 potassium channel by interaction with the actin-binding protein filamin. J Neurosci 20:8736–8744.

Reuter H (1995) Measurements of exocytosis from single presynaptic nerve terminals reveal heterogeneous inhibition by Ca^{2+}-channel blockers. Neuron 14:773–779.

Sampson LJ, Leyland ML, Dart C (2003) Direct interaction between the actin-binding protein filamin-A and the inwardly rectifying potassium channel, Kir2.1. J Biol Chem 278:41988–41997.

Scholz KP, Miller RJ (1995) Developmental changes in presynaptic calcium channels coupled to glutamate release in cultured rat hippocampal neurons. J Neurosci 15:4612–4617.

Seck T, Baron R, Horne WC (2003) Binding of filamin to the C-terminal tail of the calcitonin receptor controls recycling. J Biol Chem 278:10408–10416.

Sheng M, Pak DT (2000) Ligand-gated ion channel interactions with cytoskeletal and signaling proteins. Annu Rev Physiol 62:755–778.

Sheng ZH, Rettig J, Takahashi M, Catterall WA (1994) Identification of a syntaxin-binding site on N-type calcium channels. Neuron 13:1303–1313.

Sheng ZH, Westenbroek RE, Catterall WA (1998) Physical link and functional coupling of presynaptic calcium channels and the synaptic vesicle docking/fusion machinery. J Bioenerg Biomembr 30:335–345.

Stanley EF (1997) The calcium channel and the organization of the presynaptic transmitter release face. Trends Neurosci 20:404–409.

Szabo Z, Obermair GJ, Cooper CB, Zamponi GW, Flucher BE (2006) Role of the synprint site in presynaptic targeting of the calcium channel $Ca_V2.2$ in hippocampal neurons. Eur J Neurosci 24:709–718.

Tögel M, Wiche G, Propst F (1998) Novel features of the light chain of microtubule-associated protein MAP1B: microtubule stabilization, self interaction, actin filament binding, and regulation by the heavy chain. J Cell Biol 143:695–707.

Tombler E, Cabanilla NJ, Carman P, Permaul N, Hall JJ, Richman RW, Lee J, Rodriguez J, Felsenfeld DP, Hennigan RF, Diversé-Pierluissi MA (2006) G protein-induced trafficking of voltage-dependent calcium channels. J Biol Chem 281:1827–1839.

Wu LG, Saggau P (1997) Presynaptic inhibition of elecited neurotransmitter release. Trends Neurosci 20:204–212.